© 2020. Published by The Company of Biologists Ltd | Development (2020) 147, dev185132. doi:10.1242/dev.185132

STEM CELLS AND REGENERATION

RESEARCH ARTICLE

Heterogeneous nuclear ribonucleoprotein A3 controls mitotic progression of neural progenitors via interaction with cohesin

Min-Yi Ou[1,2,3], Xiang-Chun Ju[1,*], Yi-Jun Cai[1], Xin-Yao Sun[1,2,3], Jun-Feng Wang[2], Xiu-Qing Fu[2], Qiang Sun[1] and Zhen-Ge Luo[2,‡]

ABSTRACT

Cortex development is controlled by temporal patterning of neural progenitor (NP) competence with sequential generation of deep and superficial layer neurons, but underlying mechanisms remain elusive. Here, we report a role for heterogeneous nuclear ribonucleoprotein A3 (HNRNPA3) in regulating the division of early cortical NPs that mainly give rise to deep-layer neurons via direct neurogenesis. HNRNPA3 is expressed at high levels in NPs of mouse and human cortex at early stages, with a unique peri-chromosome pattern. Intriguingly, downregulation of HNRNPA3 caused chromosome disarrangement, which hindered normal separation of chromosomes during NP division, leading to mitotic delay. Furthermore, HNRNPA3 is associated with the cohesin-core subunit SMC1A and controls its association with chromosomes, implicating a mechanism for the role of HNRNPA3 in regulating chromosome segregation in dividing NPs. *Hnrnpa3*-deficient mice exhibited reduced cortical thickness, especially of deep layers. Moreover, downregulation of HNRNPA3 in cultured human cerebral organoids led to marked reduction in NPs and deep-layer neurons. Thus, this study has identified a crucial role for HNRNPA3 in NP division and highlighted the relationship between mitosis progression and early neurogenesis.

KEY WORDS: HNRNPA3, Cohesin, Neural progenitor division, Neocortex development, Neurogenesis

INTRODUCTION

During neocortical development, distinct subtypes of excitatory neurons are born in well-ordered temporal patterns via direct or indirect neurogenesis pathways and migrate to form multiple layers with 'inside out' manner to form deep and up layers sequentially (Angevine and Sidman, 1961; Marin-Padilla, 1978; Noctor et al., 2004; Rakic, 1974). Radial glia cells (RGs) localized in the apical ventricular zone (VZ) can undergo either symmetric proliferative division, generating two daughter RGs and expanding the progenitor pool, or asymmetric neurogenic division to produce a RG and a postmitotic neuron or an intermediate progenitor (IP) residing in the subvetricular zone (SVZ) (Haubensak et al., 2004; Malatesta et al., 2000; Miyata et al., 2004; Noctor et al., 2001, 2004). Intriguingly, several heterogeneous types of neural progenitors (NPs) with high proliferation potency, including IPs in the inner SVZ (iSVZ) and so called 'outer' or 'basal' radial glia cells (oRGs or bRGs) in the outer SVZ (oSVZ) are prominent in primates (Betizeau et al., 2013; Fietz et al., 2010; Hansen et al., 2010), and these basal progenitors (BPs) in the expanded SVZ are assumed to be associated with cortex expansion (Lui et al., 2011; Otani et al., 2016; Smart et al., 2002; Sun and Hevner, 2014). Similar to IPs, oRGs also arise from ventricular RGs (vRGs) (Ju et al., 2016; Pollen et al., 2015; Wang et al., 2011). Despite the variations in the lineage of NPs, vRGs or apical progenitors (APs) are the primary types of NPs, the division of which provides the driving force for the following cortex development process. Nevertheless, molecule mechanisms that tightly control successive NP division and temporal progression of cortical neurogenesis are not fully understood.

Cell cycle progression is one of the key determinants in NP maintenance and cortical neurogenesis (Florio and Huttner, 2014; Sun and Hevner, 2014; Taverna et al., 2014). Notably, most of the genes associated with autosomal recessive primary microcephaly (MCPH), including *MCPH1*, *CDK5RAP2* (CDK5 regulatory subunit-associated protein 2), *ASPM* (abnormal spindle-like microcephy-associated) and *WDR62* (WD-repeat-containing protein 62), encode centrosome-associated proteins that govern normal cell divisions (Jayaraman et al., 2016; Kaindl et al., 2010; Nicholas et al., 2010; Sun and Hevner, 2014). Loss of these genes in mice either singly or combinatory caused centriole duplication or chromosomal organization defects and impaired mitosis, subsequently leading to reduction in the number of NPs and in cortical size (Barrera et al., 2010; Gruber et al., 2011; Jayaraman et al., 2016; Lizarraga et al., 2010; Pulvers et al., 2010). By contrast, enhanced cell cycle re-entry in NPs has been shown to promote the expansion of the NP pool and enlarge the cortical size (Chenn and Walsh, 2002; Lange et al., 2009; Mairet-Coello et al., 2012; Nonaka-Kinoshita et al., 2013). Normal progression of NP division requires high fidelity of sister chromosome segregation. However, the molecules that are responsible for maintaining chromosome integrity during cortical NP division remain unclear.

The HNRNP family was originally identified as nuclear RNA-binding proteins and many of them are suggested to be involved in multiple cellular functions, such as mRNA processing and transport, transcription, DNA repair, and telomere maintenance, through DNA- or RNA-protein or protein-protein interactions (Dreyfuss et al., 1993; Han et al., 2010; Krecic and Swanson, 1999). Among them, HNRNPA3 is less well studied. Phenotypic data from on-line DECIPHER database (decipher.sanger.ac.uk/) suggest that *HNRNPA3* is extremely intolerant of loss-of-function variation and potentially haplo-insufficiency in populations. Notably, HNRNPA3 is highly expressed in oSVZ of developing human cortex (Miller et al., 2014). Prompted by these observations, we decided to investigate the role of HNRNPA3 in cortex development.

[1]Institute of Neuroscience, Center for Excellence in Brain Science and Intelligence Technology, Chinese Academy of Sciences, Shanghai 200031, China. [2]School of Life Science and Technology, ShanghaiTech University, Shanghai 201210, China. [3]University of Chinese Academy of Sciences, Beijing 100049, China.
*Present address: Department of Evolutionary Genetics, Max Planck Institute for Evolutionary Anthropology, Leipzig 04103, Germany.

‡Author for correspondence (luozhg@shanghaitech.edu.cn)

Z.-G.L., 0000-0001-5037-0542

Handling Editor: François Guillemot
Received 29 September 2019; Accepted 3 April 2020

Development (2020) 147, dev185132. doi:10.1242/dev.185132

We found that *HNRNPA3* is highly expressed at early stages of cortical development, in particular in RGs of mouse and human. Genetic ablation of *Hnrnpa3a* in mice prolonged mitosis of vRGs and caused a marked decrease in the production of deep layer neurons. Downregulation of HNRNPA3 in cultured human organoids also caused mitotic delay of NPs and a marked decrease in the number of RGs and their neuronal progeny. Finally, we found that HNRNPA3 is distributed in peri-chromosome regions of mitotic progenitors, and the loss or downregulation of HNRNPA3 impedes the chromosome resolution of sister chromatids of dividing NPs, probably via modulating the cohesin-association with chromosomes. These results suggest a conserved role of HNRNPA3 in the division of cortical NPs.

RESULTS

Expression of HNRNPA3 in cortical neural progenitors of mouse and human

Transcriptome analysis of prenatal human brain for principle features of different proliferative layers has led to identification of a few genes that are enriched in oSVZ compared to iSVZ, and *HNRNPA3* is one of these genes (Miller et al., 2014). In line with this result, we found that, at gestational week (GW) 16.5, HNRNPA3 is highly expressed in cells at oSVZ and VZ regions compared with that in iSVZ (Fig. 1A,B). Notably, HNRNPA3 was more frequently observed in early ($PAX6^+TBR2^-$) and late ($PAX6^+TBR2^+$) RGs than in IPs ($PAX6^-TBR2^+$) in either VZ or SVZ regions (Fig. 1B,C), and many RGs labeled by HOPX also expressed HNRNPA3 in VZ and SVZ regions of human fetal cortex (Fig. 1D), and cultured cerebral organoids (Fig. S1A). To analyze the expression of *HNRNPA3* in various types of NPs and differentiated neurons, we analyzed accessible online datasets of single cell RNA-sequencing (scRNA-seq) information with reads covering full-length RNA from human fetal brain and cultured cerebral organoids (Camp et al., 2015), and extracted data using methods described previously (Kageyama et al., 2018). We found that vRGs, APs and BPs exhibit higher expression of *HNRNPA3* compared with differentiated neurons in the fetal brain (Fig. S1B) and in cultured organoids (Fig. S1C). Further analysis of dynamic expression patterns of individual genes, as reported recently (Camp et al., 2015; Kageyama et al., 2018; Telley et al., 2016), indicates that *HNRNPA3* shares parallel expression waves with *PCM1*, which is involved in centromere assembly, and this pattern is conserved in mouse and human fetal brain, and in cultured human cerebral organoids (Fig. S1D). The gradual decrease in the level of *PAX6* and increase in *DCX*, a marker for differentiated newborn neurons, indicates reliability of the analysis. Unlike *HNRNPA3*, the close subfamily member *HNRNPA1* displayed ubiquitous expression throughout development, in particular in human fetal brain (Fig. S1D).

In rodents, RGs are the major cortical NPs that can undergo multiple rounds of proliferative divisions and IPs can undergo only one round of neurogenic division (Haubensak et al., 2004; Miyata et al., 2004; Noctor et al., 2004). Interestingly, temporal expression patterns of pulse-labeled apical progenitors and their daughter cells reported in a recent study (Telley et al., 2019) revealed that *Hnrnpa3* was expressed at higher levels in APs at early neurogenesis stage than at later stages (Fig. S1E). Indeed, scRNA-seq data showed that *Hnrnpa3* exhibited the highest expression in RGs and then declined in IPs and post-mitotic neurons (Fig. S1F) (Telley et al., 2016). Consistent with gene expression patterns, the level of Hnrnpa3 protein also gradually decreased from E12.5 to E15.5 in VZ and SVZ regions (Fig. 1E). In line with this notion, we detected high levels of Hnrnpa3 signal in $Pax6^+Tbr2^-$ RGs in the VZ region and relatively low levels in $Pax6^-Tbr2^+$ IPs in both the VZ or SVZ of mice at E13.5 (Fig. 1F). Taken together, the expression level of *HNRNPA3* is positively associated with cortical NPs with higher proliferation potency.

Hnrnpa3a deletion impaired cortical development in mice

It has been reported that there are two protein isoforms derived from *Hnrnpa3* – a longer *Hnrnpa3a* isoform and a shorter *Hnrnpa3b* isoform – and the a-isoform predominates in human tissues (Papadopoulou et al., 2012). As shown in Fig. S1G, Hnrnpa3a was widely expressed in various tissues, including cerebrum, cerebellum, lung, pancreas and spinal cord, whereas Hnrnpa3b was expressed in limited tissues such as cerebrum, kidney and skeletal muscle. To investigate whether *Hnrnpa3* is involved in cortical development, we took advantage of CRISPR/Cas9-mediated genome editing to generate *Hnrnpa3a* knockout (KO) mice (Fig. 2A). For this purpose, sgRNA was designed to target *Hnrnpa3a* at exon 1, which is absent in *Hnrnpa3b* (Fig. 2A). Compared with wild-type (WT) littermates, homozygous *Hnrnpa3a* KO mice showed marked reduction in the level of Hnrnpa3a, but not Hnrnpa3b, in the brain at E14.5 (Fig. 2B). Notably, the *Hnrnpa3a* KO mice exhibited barely detectable levels of Hnrnpa3 protein in VZ/SVZ regions (Fig. 2C), suggesting that Hnrnpa3a is the major isoform expressed in cortical NPs. Although there was no apparent abnormality in the morphology of whole body and the brain (Fig. S2A,B), the *Hnrnpa3a* KO mice died shortly after birth, probably owing to neonatal hypoxia caused by lung developmental defects (Fig. S2A,D,E). The neuromuscular synapses in the diaphragm were roughly normal (Fig. S2C).

Next, we determined cortical lamination by staining with layer V marker Ctip2 and layer II-IV marker Cux1 in mice at P0. We found that the *Hnrnpa3a* KO mice exhibited a mild but significant reduction in the thickness of the dorsal lateral cortex compared with that of wild-type littermates (Fig. 2D,E). Notably, the layer thickness and numbers of $Ctip2^+$ cells, but not that of $Cux1^+$ cells, were reduced in *Hnrnpa3a* KO mice (Fig. 2F-I). Consistent with this result, *Hnrnpa3a* KO mice at E18.5 also displayed a significant reduction of early formed layer VI labeled by Tbr1 (Fig. 2J-L). The number of Tbr2-labeled IP cells, which give rise to superficial layer neurons, was similar in wild-type and KO mice at E14.5 (Fig. 2M,N). Thus, Hnrnpa3a plays an important role in the neurogenesis of cortical neurons, in particular of $Ctip2^+$ deep layer neurons. The specific effects on early-born deep layer neurons might be attributable to the temporal high level expression of Hnrnpa3a in RGs at early stages of cortex development.

Hnrnpa3a ablation leads to mitotic retardation in apical cortical progenitors

In light of aforementioned findings, we next asked whether the loss of Hnrnpa3a affected the proliferation or differentiation process of NPs. First, we used an antibody against phosphorylated histone 3 (PH3) to label mitotic cells in mice at various embryonic stages. We found that the number of $PH3^+$ cells was similar in wild-type and *Hnrnpa3a* KO mice at E12.5, but markedly increased in *Hnrnpa3a* KO mice at later stages at E14.5 or E17.5 (Fig. 3A-D). Interestingly, unlike wild-type $PH3^+$ cells that were aligned and attached to apical surface of the VZ, many $PH3^+$ cells were stacked to form clusters at the VZ regions in *Hnrnpa3a* KO mice at E14.5 (Fig. 3E). By judging chromosome arrangement according to distribution of DAPI signals in dividing cells marked by phosphorylated-vimentin (p-Vim) (Insolera et al., 2014), we measured the proportions of VZ

Development (2020) 147, dev185132. doi:10.1242/dev.185132

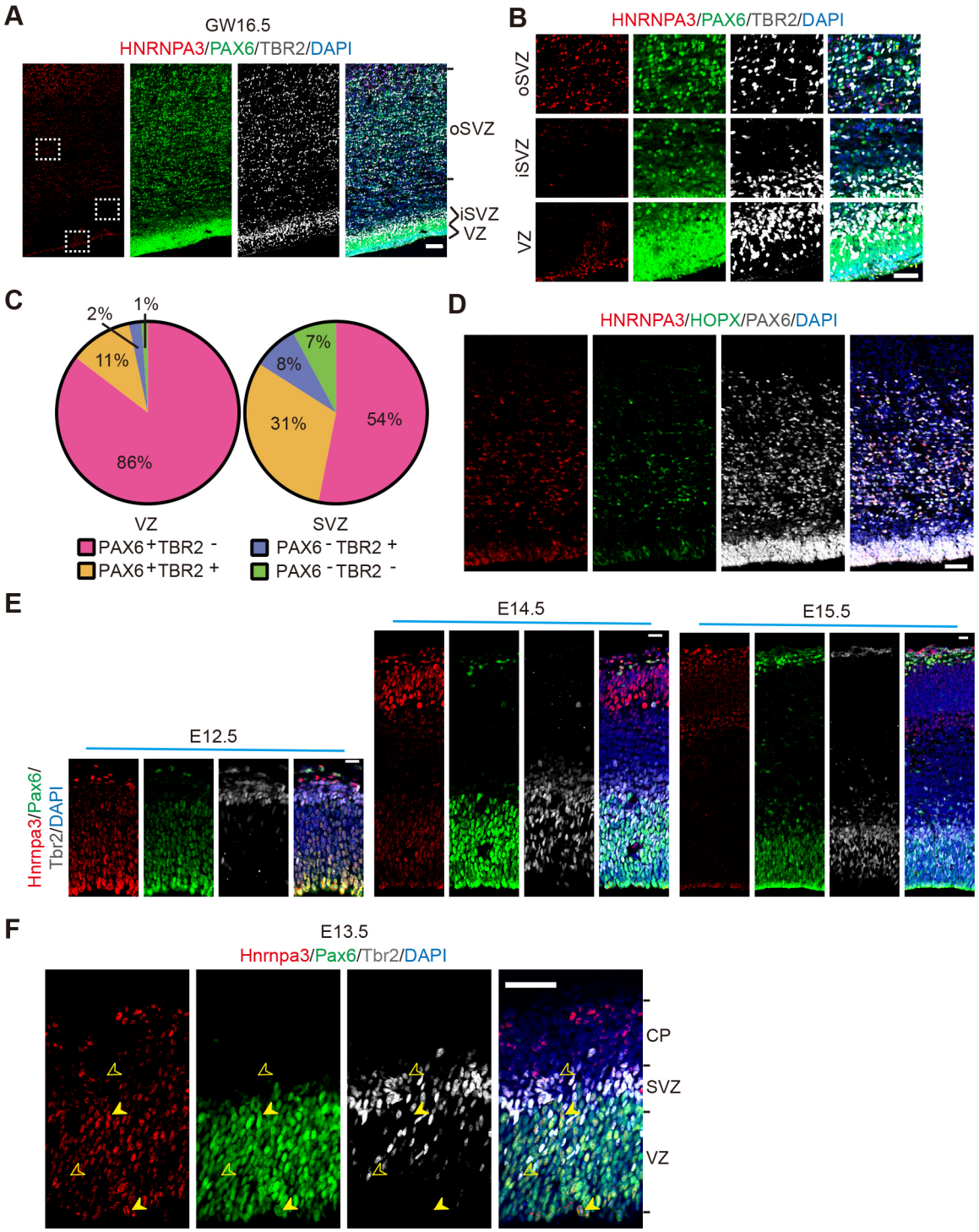

Fig. 1. Expression of HNRNPA3 in neural progenitors in mouse and human samples. (A,B) GW16.5 human fetal brain slices were immunostained with antibodies against HNRNPA3 (red), PAX6 (green) and TBR2 (gray), using DAPI to mark cell nuclei. VZ, the ventricular zone; iSVZ, inner subventricular zone; oSVZ, outer subventricular zone. Scale bars: 100 µm in A; 50 µm in B. (C) Percentage distribution of subpopulations of HNRNPA3^{+} cells in the human VZ and SVZ regions at GW16.5. (D) Immunostaining of GW16.5 human fetal brain slices using antibodies against HNRNPA3 (red), HOPX (green) and PAX6 (gray), using DAPI to label cell nuclei. Scale bar: 50 µm. (E) Immunostaining for Hnrnpa3 (red), Pax6 (green) and Tbr2 (gray) in brain slices from mice at E12.5, E14.5 or E15.5. Scale bars: 20 µm. (F) Brain slices from E13.5 mice were immunostained using antibodies against Hnrnpa3 (red), Pax6 (green) and Tbr2 (gray), together with DAPI (blue). Solid arrowheads indicate Pax6^{+} Tbr2^{-} cells. Hollow arrowheads indicate Pax6^{-} Tbr2^{+} cells. Scale bar: 50 µm.

cells in different phases of mitosis, and found that *Hnrnpa3a* KO mice at E12.5 exhibited marked increase in the percentage of cells in prophase and pro-metaphase (pro/pro-metaphase) (Fig. 3F,G). These results suggest that the increase and abnormal distribution of mitotic cells might be due to cell cycle arrest. To further consolidate this conclusion, we pulse-labeled cycling NPs by BrdU injection at E12.5 and analyzed the percentage of PH3^{+}BrdU^{+} cells among the BrdU^{+} cells, which represents cells arrested in mitosis

Development (2020) 147, dev185132. doi:10.1242/dev.185132

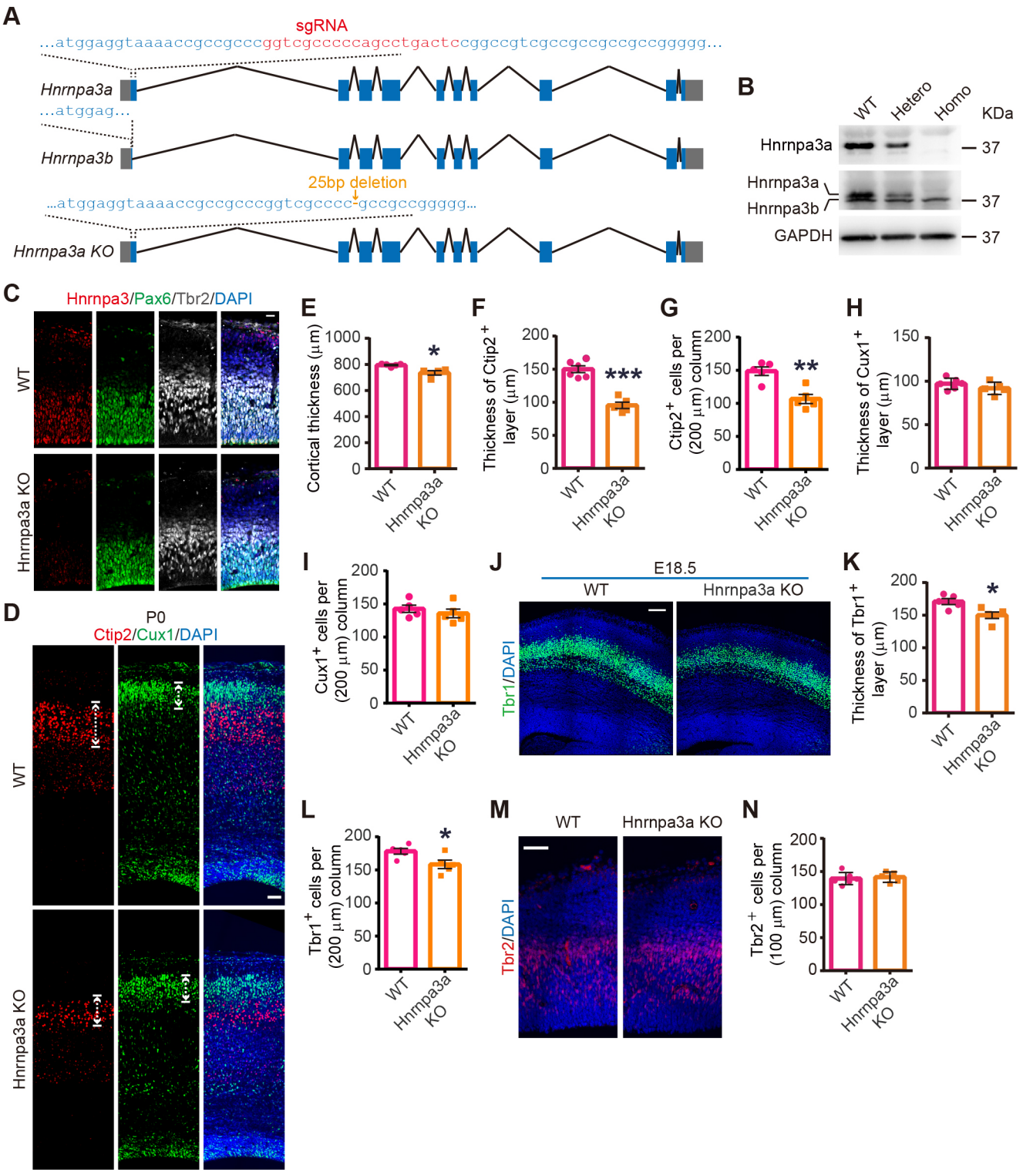

Fig. 2. See next page for legend.

(Ye et al., 2017). The increased mitotic index in *Hnrnpa3a* KO mice also suggests delayed mitotic progression in NPs (Fig. 3H,I).

Next, we measured the proportion of mitotic cells, which displayed condensed Ki67 full labeling associated with the chromosome, among the Ki67^{+} cycling progenitors, according to the methods described previously (Betizeau et al., 2013; Pilaz et al., 2016) (Fig. 3J,K). Although total numbers of proliferative RGs were similar between wild-type and *Hnrnpa3a* KO mice at E14.5 (Fig. 3L), the percentage of RGs at mitotic phase was increased in *Hnrnpa3a* KO mice (Fig. 3M), indicating again a mitotic delay.

To directly observe the cell division process, we performed live imaging of mitotic RGs in cultured brain slices from mice at E13.5 (Fig. 4A). We found that the percentage of RGs with prolonged M-phase duration was higher in *Hnrnpa3a* KO mice than in

Development (2020) 147, dev185132. doi:10.1242/dev.185132

Fig. 2. Cortical developmental defects in *Hnrnpa3a* knockout mice. (A) *Hnrnpa3a* knockout mice were generated by CRISPR/Cas9-mediated genome editing on exon1 of *Hnrnpa3a*. The targeted sequence is highlighted in red, which is present in *Hnrnpa3a* but absent in *Hnrnpa3b*. Blue boxes indicate individual exons linked by introns (black lines). (B) Homogenates of brain samples from E14.5 mice were subjected to immunoblot using antibodies against Hnrnpa3a (top row), Hnrnpa3 (middle row) or GAPDH (bottom row). (C) Brain slices from mice at E13.5 were immunostained using antibodies against Hnrnpa3 (red), Pax6 (green) and Tbr2 (gray), together with DAPI (blue) staining. Scale bar: 20 µm. (D) Brain slices from mice at P0 were immunostained using antibodies against Cux1 (green) and Ctip2 (red) with DAPI (blue) marking cell nucleus. Scale bar: 50 µm. Arrows indicate where thickness measurements were made. (E) Quantification of the cortical thickness of mice at P0 (Kolmogorov–Smirnov test, $^{*}P$=0.0159). (F,G) Quantification of the thickness of the Ctip2^{+} cell layer (F, unpaired *t*-test, $^{***}P$<0.0001) or the number of Ctip2^{+} cells (G, unpaired *t*-test, $^{**}P$=0.0021). (H,I) Quantification of the thickness of Cux1^{+} cell layer (H, unpaired *t*-test, P=0.2296) or the number of Cux1^{+} cells at P0 (I, unpaired *t*-test, P=0.4355). (J) Brain slices from E18.5 mice were immunostained using Tbr1 antibody (green) and DAPI (blue). Scale bar: 100 µm. (K,L) Quantification of the thickness of the Tbr1^{+} cell layers (K, unpaired *t*-test with Welch's correction, $^{*}P$=0.0148) or number of Tbr1^{+} cells at E18.5 (L, unpaired *t*-test, $^{*}P$=0.0341). (M) Brain sections of E14.5 wild-type or *Hnrnpa3a* KO mice were stained for Tbr2 (red) and with DAPI (blue). Scale bar: 50 µm. (N) Quantification for the number of Tbr2^{+} progenitors (unpaired *t*-test, P=0.6760).

wild-type mice (Fig. 4B), providing direct evidence that loss of *Hnrnpa3a* impeded RG division by causing mitotic delay.

Early NPs in the mouse VZ can undergo proliferative symmetrical divisions if they occur in a vertical cleavage plane relative to the VZ surface or self-consumptive asymmetrical divisions if they occur in a horizontal plane (Mora-Bermúdez and Huttner, 2015; Sun and Hevner, 2014). Based on distribution patterns of chromosomes in mitotic RGs, we analyzed division angles of RGs at VZ regions of wild-type and KO mice (Fig. 4C). We found that NPs in *Hnrnpa3a* KO mice displayed a notable increase in oblique division (30-60°) at the cost of near-vertical division (60-90°) (Fig. 4C,D). The changes in cleavage plane relative to VZ surface might be due to mis-arrangement of chromosomes and subsequent disruption of spindle apparatus.

It has been reported that NPs with prolonged mitosis are usually committed to apoptosis or accelerated neurogenic competence (Pilaz et al., 2016). However, the *Hnrnpa3a* KO mice did not exhibit apparent apoptosis at least at the time of our observation (Fig. S3A-C), although DNA damage response reflected by the signals of γH2AX, which marks DNA damage-driven histone modification, was evoked in KO mice (Fig. 4E,F). The activation of DNA repair pathway, which was measured by phosphorylated-Atm (pS1981) (Fig. 4G,H), may have protected cells from death. Thus, the loss of *Hnrnpa3a* hindered neurogenic cell division of early NPs and impaired neuronal competency.

Downregulation of *Hnrnpa3* causes abnormal chromosome arrangement

The protracted mitosis of RGs in *Hnrnpa3a* KO mice prompted us to determine subcellular distribution of Hnrnpa3 in mitotic cells. Interestingly, we found that Hnrnpa3 was enriched in peri-chromosome regions, especially in regions between two sister chromosomes of dividing NPs in the VZ (Fig. 5A, top lane). The signal was specific for Hnrnpa3a, because it was not observed in *Hnrnpa3a* KO mice (Fig. 5A, bottom row). Interestingly, much more NPs of *Hnrnpa3a* KO mice exhibited chromatin bridges at anaphase, as shown in fixed samples (Fig. 5B,C) and in live imaging of cultured brain slices (Fig. 5D). Notably, the NPs with chromatin bridges still finished the mitotic process, and finally gave rise to two daughter cells, although this process was abnormally prolonged (Fig. 5D). In addition to chromatin bridges, many mitotic NPs in KO mice also exhibited chromosome fragments (Fig. 5E), which might be derived from chromosome mis-alignment or mis-segregation, as shown previously (Crasta et al., 2012).

Next, we determined the HNRNPA3 localization and functions in human neural stem cells. In the human neural stem cell ReN at M-phase, HNRNPA3 was also distributed in peri-chromosome regions (Fig. S4A). However, upon treatment with nocodazole, which was used to induce cell division arrest by causing microtubule depolymerization and spindle disassembly, HNRNPA3 was segregated from the peri-chromosome regions (Fig. S4A). In mitotic ReN cells transfected with construct encoding small interference RNA against HNRNPA3 (shA3), which was able to downregulate the expression of *HNRNPA3* (Fig. S4B), the percentage of cells exhibiting chromosome misalignment and spindle disorganization was dramatically increased compared with control cells transfected with construct encoding scrambled sequence (shScr) (Fig. S4C,D). These phenomena were unlikely to be caused by impairment of spindle assembly checkpoint activity, because the crucial mitotic checkpoint protein BUB-related 1 (BubR1) remained associated with chromosomes in HNRNPA3 knockdown ReN cells at prometaphase (Fig. 6A). Chromosome segregation errors can trigger the formation of DNA breaks that may evoke DNA damage responses (Crasta et al., 2012). Indeed, ReN cells with HNRNPA3 knockdown exhibited marked increase in the levels of γH2AX revealed by either immunostaining or immunoblotting (Fig. S4E,F).

As a RNA-binding protein, how does HNRNPA3 regulate chromosome organization during mitosis? In dividing cells, sister chromatids are held together by cohesin complexes, which are then removed from DNA during prometaphase, and the cohesion release is necessary for the separation of sister chromatids (Haarhuis et al., 2014). Notably, HNRNPA3 was found in a protein complex containing cohesion proteins, including the structural maintenance of chromosomes 1 (SMC1) – a key component of cohesin complex, which has been shown to be needed for mitotic progression (Yeh et al., 2015; Ma et al., 2013). As shown in Fig. 6B, immunoprecipitation (IP) using SMC1A antibody caused co-IP of HNRNPA3 in the lysates of ReN cells, confirming their association. In ReN cells at prophase, SMC1A was associated with chromosomes, where it was largely colocalized with Hnrnpa3a tagged with EGFP (Fig. 6C). During the transition from prophase to metaphase, SMC1A is gradually released from chromosomes, then associated with bipolar spindle apparatus and finally recruited to bipolar centromeric spindle pole (Guan et al., 2008; Wong and Blobel, 2008). The phosphorylation of cohesin complex proteins, including SMC1A, has been shown to stimulate their release from chromosomes and then binding to spindle apparatus (Nishiyama et al., 2013; Sumara et al., 2002; Wong and Blobel, 2008). Intriguingly, HNRNPA3 knockdown ReN cells exhibited a reduced level of phosphorylated SMC1A (p-SMC1A), which was localized in centrosomes labeled by γ-tubulin at prometaphase (Fig. 6D,E). Unlike control cells that showed SMC1A association with spindle, extensive SMC1A signals still remained attached to chromosomes in HNRNPA3 knockdown cells at metaphase (Fig. 6F). These results suggest that HNRNPA3 modulates dynamic association of cohesin with chromosomes and spindle apparatus to precisely control chromosome segregation during cell division.

Role of Hnrnpa3a in early direct neurogenesis in mice

To further determine the outcomes of mitotic delay caused by the loss of Hnrnpa3a in mice, we pulse labeled cycling NPs by BrdU injection at E12.5 or E14.5 and analyzed cell cycle exit and re-entry after 24 h by

Development (2020) 147, dev185132. doi:10.1242/dev.185132

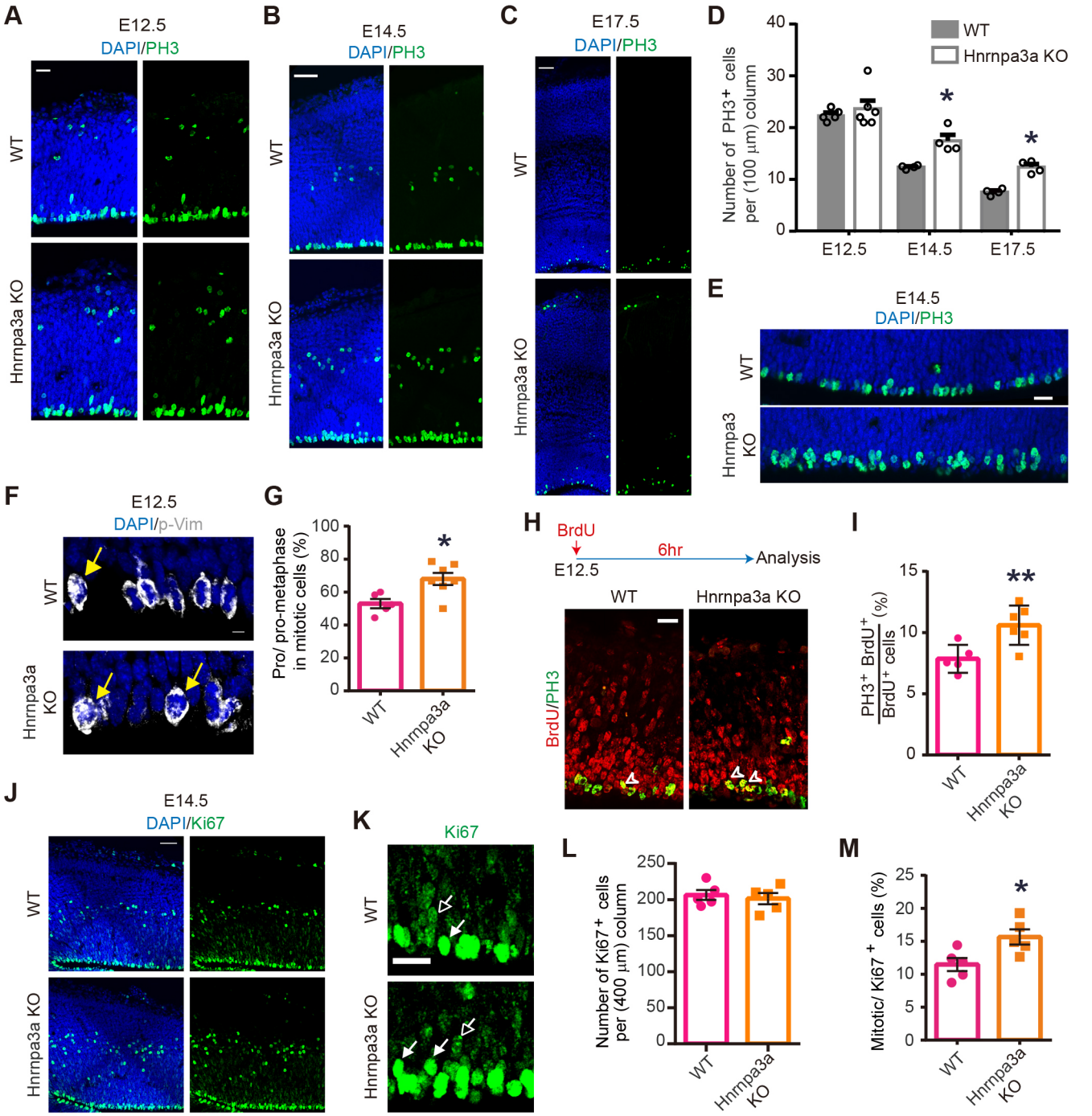

Fig. 3. Mitotic arrest of cortical neural progenitors in *Hnrnpa3a* knockout mice. (A-C) Brain slices from mice at indicated embryonic days (E12.5, E14.5 and E17.5) were stained using PH3 antibody (green) and with DAPI (blue). Scale bars: 20 µm in A; 50 µm in B,C. (D) Quantification of PH3-positive cells at E12.5 (unpaired *t*-test with Welch's correction, P=0.468), E14.5 (Mann–Whitney test, *P=0.0286) and E17.5 (Mann–Whitney test, *P=0.0286). (E) Distribution of PH3$^+$ cells (green) in VZ regions from wild-type or KO mice at E14.5. Scale bar: 20 µm. (F) Immunostaining for phospho-vimentin (p-Vim, gray) in the VZ region of E12.5 mice. Yellow arrows indicate cells at pro/pro-metaphase exhibiting compact chromosome and p-Vim signals. Scale bar: 5 µm. (G) Quantification of mitotic cells in pro/pro-metaphase phase (unpaired *t*-test, *P=0.0135). At least five embryos were analyzed in each group. (H) E12.5 mice were pulse labeled by BrdU and examined 6 h later by staining using antibodies against BrdU (red) and PH3 (green). Scale bar: 20 µm. (I) Quantification of the percentage of PH3$^+$BrdU$^+$ cells among BrdU$^+$ cells (unpaired *t*-test with Welch's correction, **P=0.0095). (J) Immunostaining for Ki67 signals (green) in mice at E14.5. Scale bar: 50 µm. (K) Different types of Ki67 labeling. Solid arrows indicate mitotic cycling cells with condensed Ki67 labeling in nuclei. Hollow arrows indicate cycling cells out of mitosis with diluted Ki67 signals. Scale bar: 20 µm. (L) Quantification of total cycling NPs in mice at E14.5 (unpaired *t*-test, P=0.6462). Five embryos were analyzed in each group. (M) Quantification of mitotic Ki67$^+$ NPs in E14.5 cortices (unpaired *t*-test, *P=0.0254).

immunostaining with cell cycling marker Ki67. Notably, with BrdU injection at E12.5, the percentage of BrdU$^+$Ki67$^-$ cells among total BrdU$^+$ cells was significantly decreased in E13.5 *Hnrnpa3a* KO mice compared with wild-type littermates (Fig. 7A,B), suggesting a reduction in NP progeny that had left the cell cycle. However, this phenomenon was not observed in E15.5 *Hnrnpa3a* KO mice after BrdU pulse labeling at E14.5 (Fig. S5A,B). Furthermore, the percentage of BrdU$^+$Ki67$^+$ cells among Ki67$^+$ cells was decreased

Development (2020) 147, dev185132. doi:10.1242/dev.185132

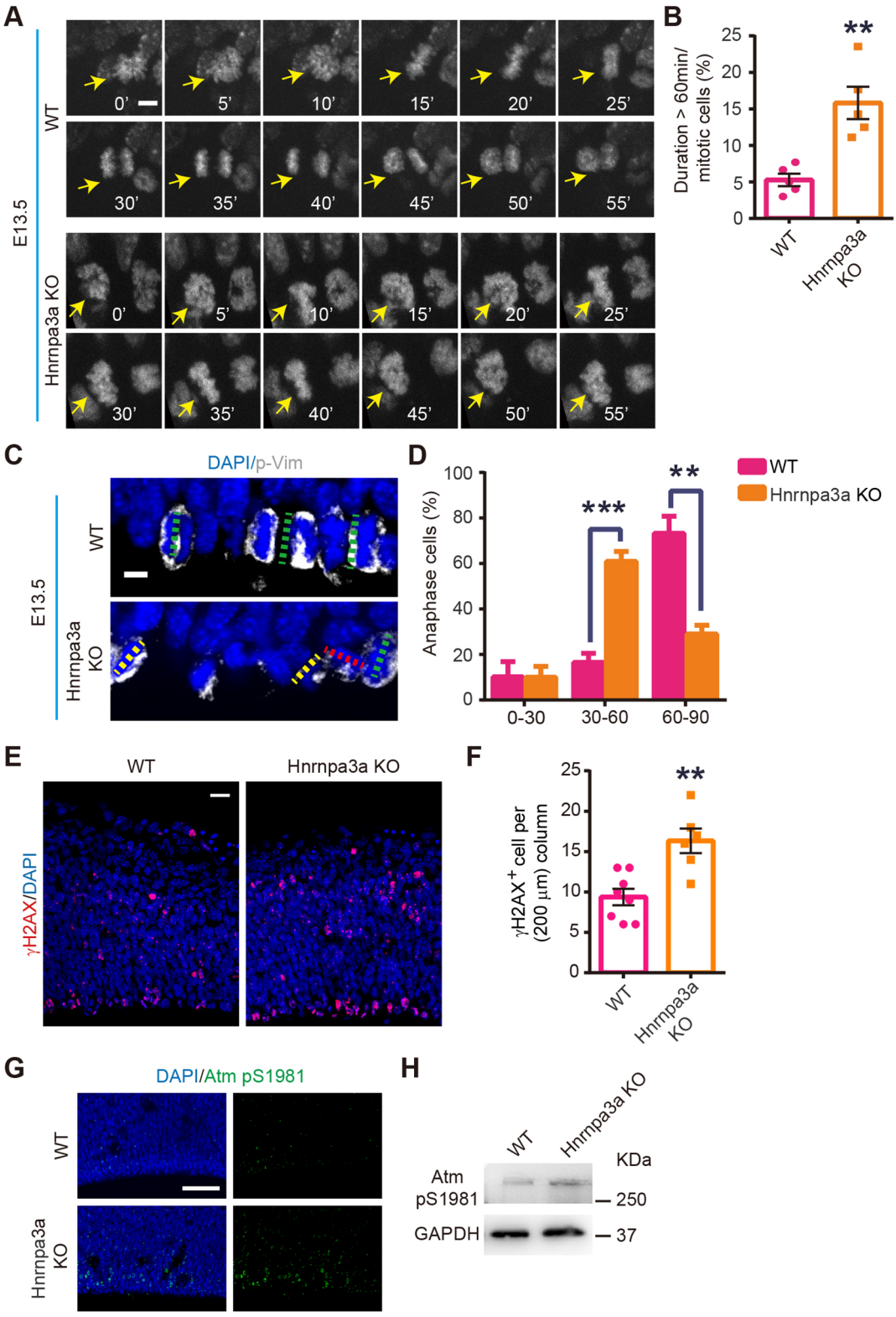

Fig. 4. Hnrnpa3a deficiency prolongs NP division and promotes DNA damage response. (A) Live imaging for mitotic processes of APs in brain slices from E13.5 mice of indicated genotypes. Hoechst was used to label DNA. Scale bar: 5 µm. (B) Quantification for the percentage of cells with a mitotic duration of more than 60 min of the indicated genotypes (unpaired *t*-test with Welch's correction, $^{**}P$=0.0063). (C) Division orientation of p-Vim^{+} (gray) APs from wild-type or KO mice at E13.5. DAPI was used to mark chromosome structure and distributions and division plates are delineated by dotted lines: red, 0-30°; yellow, 30-60°; green, 60-90°. Scale bar: 5 µm. (D) Quantification of the percentage of APs at anaphase with indicated division angles. Data are mean±s.e.m. (n=6 mice for wild type; n=7 for KO; 0-30°, P>0.9; 30-60°, $^{***}P$=0.0006; 60-90°, $^{**}P$=0.0017, Mann–Whitney test). (E) Brain slices from E13.5 mice were stained for γH2AX (red) and with DAPI (blue). Scale bar: 20 µm. (F) Quantification of the number of γH2AX^{+} cells in mice of indicated genotype (unpaired *t*-test, $^{**}P$=0.0019). (G) Immunostaining for the signals of phosphorylated-Atm (pS1981) in VZ/SVZ regions of E13.5 mice of the indicated genotype. Scale bar: 50 µm. (H) Immunoblotting for the level of phosphorylated-Atm (pS1981) in the homogenates of E14.5 mice brain, using GAPDH as an internal control.

Development (2020) 147, dev185132. doi:10.1242/dev.185132

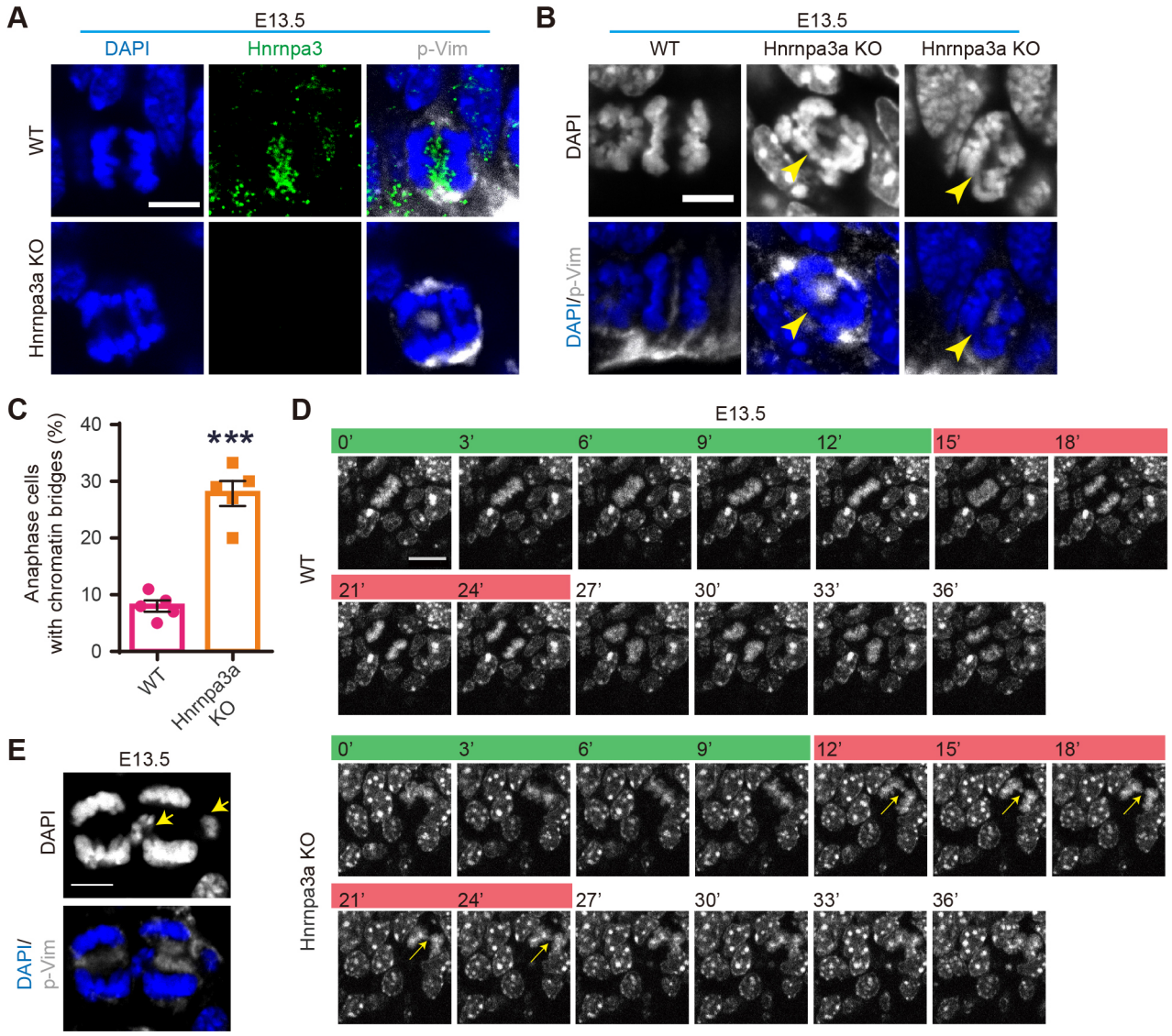

Fig. 5. Loss of Hnrnpa3a impairs segregation of sister chromatids of NPs. (A) Expression of Hnrnpa3 (green) in apical progenitors (APs) at VZ regions of wild-type or KO mice at E13.5. Scale bar: 10 µm. (B) Immunostaining with p-Vim antibody to mark mitotic APs in mice at E13.5. There are chromatin bridges (yellow arrowheads) in APs of KO mice. Scale bar: 10 µm. (C) Quantification of the percentage of anaphase cells with chromatin bridges (unpaired *t*-test with Welch's correction, ***P=0.0003). Five embryos were analyzed in each group. (D) Brain slices from mice at E13.5 were labeled with Hoechst, followed by time-lapse imaging for the segregation progress of sister chromatids during AP division. Chromatin bridges (yellow arrows) and prolonged anaphase are present in KO mice. Mitotic stages are indicated above each panel (green, metaphase; red, anaphase). Scale bar: 10 µm. (E) Immunostaining of p-Vim and DAPI of APs in KO mice at E13.5. The chromosome fragments and micronuclei are indicated by yellow arrows. Scale bar: 10 µm. Five embryos were analyzed in each group.

in *Hnrnpa3a* KO mice at E13.5 (BrdU injection at E12.5) (Fig. 7C), but not E15.5 (BrdU injection at E14.5) (Fig. S5C). Thus, the effects on cell cycle progression caused by the loss of *Hnrnpa3a* may be limited to NPs at early periods. To directly trace the cell cycle re-entry of progenitors after division, we labeled the mitotic cells with carboxyfluorescein esters (CFSE) injected at E12.5 followed by an EdU pulse 1 day later (Fig. 7D). We found that *Hnrnpa3a* KO mice displayed a marked reduction in the percentage of mitotic progenitors that entered a new round of the cell cycle (Fig. 7E). The decrease in cell cycle re-entry was most likely caused by mitotic delay, as mentioned above.

We then asked whether the mitotic delay had any effect on neuronal fates. To this end, we performed immunostaining for new-born neuronal marker Dcx at E13.5 after CFSE injection at E12.5. We found the percentage of $Dcx^{+}CSFE^{+}$ cells, which represents neuronal progeny via direct neurogenic division, was decreased in *Hnrnpa3a* KO mice compared with wild-type littermates (Fig. 7F,G). This result suggests that the loss of *Hnrnpa3a* in NPs impairs neuronal progeny. To further assess the effects of *Hnrnpa3a* ablation on neuronal specification, we analyzed neuronal fates in mice at P0 after BrdU pulse at E12.5, by calculating the percentage of cells labeled by pan-neuronal marker NeuN, or layer marker Ctip2 or Cux1, among cells with fully retained BrdU ($BrdU^{full}$), which were considered as daughter neurons directly derived from NPs after the last round of division (Cárdenas et al., 2018) (Fig. 7H-K and Fig. S5D,E). We found that the percentage of $Ctip2^{+}BrdU^{full}$ among $BrdU^{full}$ cells was significantly decreased in *Hnrnpa3a* KO mice compared with wild-type littermates (Fig. 7H,J), whereas the percentage of $Cux1^{+}BrdU^{full}$ or $NeuN^{+}BrdU^{full}$ among $BrdU^{full}$ cells had no difference (Fig. 7H,K; Fig. S5D,E). These results support the conclusion that mitotic delay caused by the loss of *Hnrnpa3a* impairs early neurogenesis rather than neuronal fate specification.

Development (2020) 147, dev185132. doi:10.1242/dev.185132

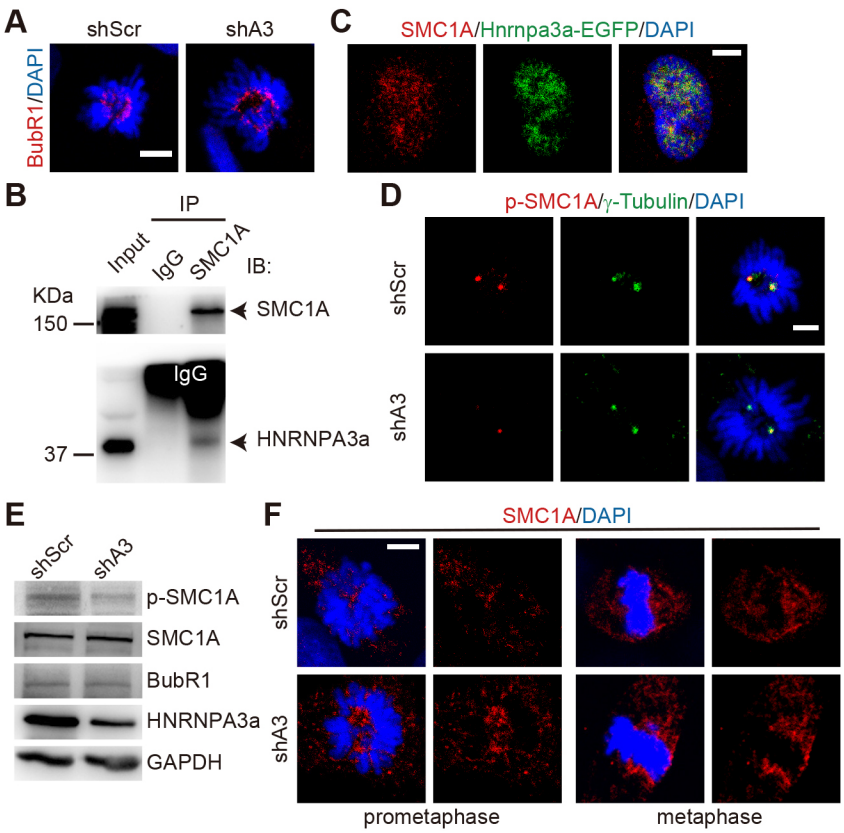

Fig. 6. HNRNPA3 is associated with cohesin in mitotic NPs. (A) Immunostaining for BubR1 localization in control (shScr) or HNRNPA3 knockdown (shA3) ReN cells at prometaphase with DAPI marking chromosomes. Scale bar: 5 µm. (B) Cell lysates of ReN cells were subjected to immunoprecipitation (IP) with SMC1A antibody or control IgG, followed by immunoblotting with SMC1A or HNRNPA3a antibody. Data are representative of the results of three independent experiments. (C) Localization of HNRNPA3a-EYFP (green) and endogenous SMC1A (red) in ReN cells at prophase. Scale bar: 5 µm. (D) Immunostaining for the signals of phosphorylated SMC1A (p-SMC1A, red) and γ-tubulin (green) in control or HNRNPA3 knockdown ReN cells at prometaphase. Scale bar: 5 µm. (E) Cell lysates of ReN cells transfected with shScr or shA3 were subjected to immunoblotting with the indicated antibodies. Data are representative of three independent experiments. (F) Immunostaining for the localization of SMC1A in control (shScr) or HNRNPA3 knockdown (shA3) ReN cells at prometaphase or metaphase. Scale bar: 5 µm.

To determine whether Hnrnpa3 acts cell autonomously in NPs, E12.5 mice were subjected to *in utero* electroporation (IUE) with vectors encoding shRNA against Hnrnpa3 (shA3) or scrambled sequence (shScr), together with GFP plasmid to label transfected cells, and observed at E16.5 for neuronal fates (Fig. 8A). We found that the percentage of Ctip2$^+$ cells in transfected GFP$^+$ cells was markedly reduced in shA3 mice compared with shScr control mice (Fig. 8A,B), whereas the percentage of superficial layer neurons labeled by Satb2 in GFP$^+$ cells had no difference (Fig. 8A,C). Notably, the majority of shA3-expressing neurons were localized in regions beneath the Ctip2$^+$ cell band (Fig. 8A). This migration delay might be due to neurogenesis retardation. To further consolidate this conclusion at the single clone level, we analyzed the clone trajectory of individual RGs, which were sparsely labeled at E12.5 with low-titer retrovirus expressing shA3 or control sequence together with GFP (Fig. 8D). We found a marked reduction in Ctip2$^+$ neurons and an arrest of NPs at the VZ of mice at E16.5 (Fig. 8D,E). These results suggest a cell-autonomous effect of Hnrnpa3 on the neurogenesis of early born neurons in mice. In line with a positive association between the level of Hnrnpa3 and NP stemness, overexpression (OE) of Hnrnpa3a in E14.5 mice via IUE caused an increase in Pax6-labeled RG cells in E16.5 mice (Fig. 8F,G). Furthermore, HNRNPA3 OE in ReN cells promoted cell proliferation as measured by EdU incorporation (Fig. S6A,B). Thus, the level of HNRNPA3 expressed in NPs is positively associated with mitotic progression.

Role of HNRNPA3 in the development of human cerebral organoids

Next, we investigated roles of HNRNPA3 in human cortex development by using the cerebral organoid culture system, which has been developed to mimic cortex development and related diseases (Lancaster and Knoblich, 2014). Embryonic bodies (EBs) were derived from H9 human embryonic stem cells infected by lentivirus encoding doxycycline-inducible expression of RFP reporter and shA3 or a control sequence (Ctrl) (Fig. S7A,B), following the protocol introduced previously (Li et al., 2017). To avoid potential effects on early pluripotent stages, the expression of shA3 or shCtrl was turned on at the stage of neural induction (around day 12) by adding doxycycline (1 µg/ml) to the culture medium (Fig. S7A,C), and development of cerebral organoids was examined at different days after neural induction (Fig. S7D,E). Compared with control organoids, shA3-expressing organoids displayed apparent reduction in PAX6-labeled RGs, as well as TBR2-labeled IPs (Fig. 9A,F and Fig. S7D). The defects seemed to be more severe at later stages (day 52 and day 78) than early stages (day 33) (Fig. 9A,F and Fig. S7D). Besides, the thickness of neuroepithelium composed of PAX6$^+$ cells akin to VZ-like apical surface was also decreased in *HNRNPA3* knockdown organoids compared with vehicle control organoids at D33 (Fig. 9B). With the extension of organoids culture, the overall size of the *HNRNPA3* knockdown organoids was also smaller than controls (Fig. S7E). Remarkably, deep layer neurons were largely abolished in *HNRNPA3* knockdown organoids (Fig. 9F), although residue differentiated NeuN$^+$ neurons were present (Fig. 9G). This result is consistent with the notion that the *Hnrnpa3* defect specifically affected early born deep layer neurons in mice.

We also examined the proportion of cycling NPs that remained at M phase by calculating the percentage of mitotic PH3$^+$ cells among KI67$^+$ cycling cells, and found that the *HNRNPA3* knockdown organoids displayed a marked increase in mitotic NPs (Fig. 9D,E), although total number of KI67$^+$ cells had little difference (Fig. 9C). Given that *HNRNPA3* was also highly expressed in BPs of human fetal brains (Fig. S1B,C), we examined the number of cells labeled by

Development (2020) 147, dev185132. doi:10.1242/dev.185132

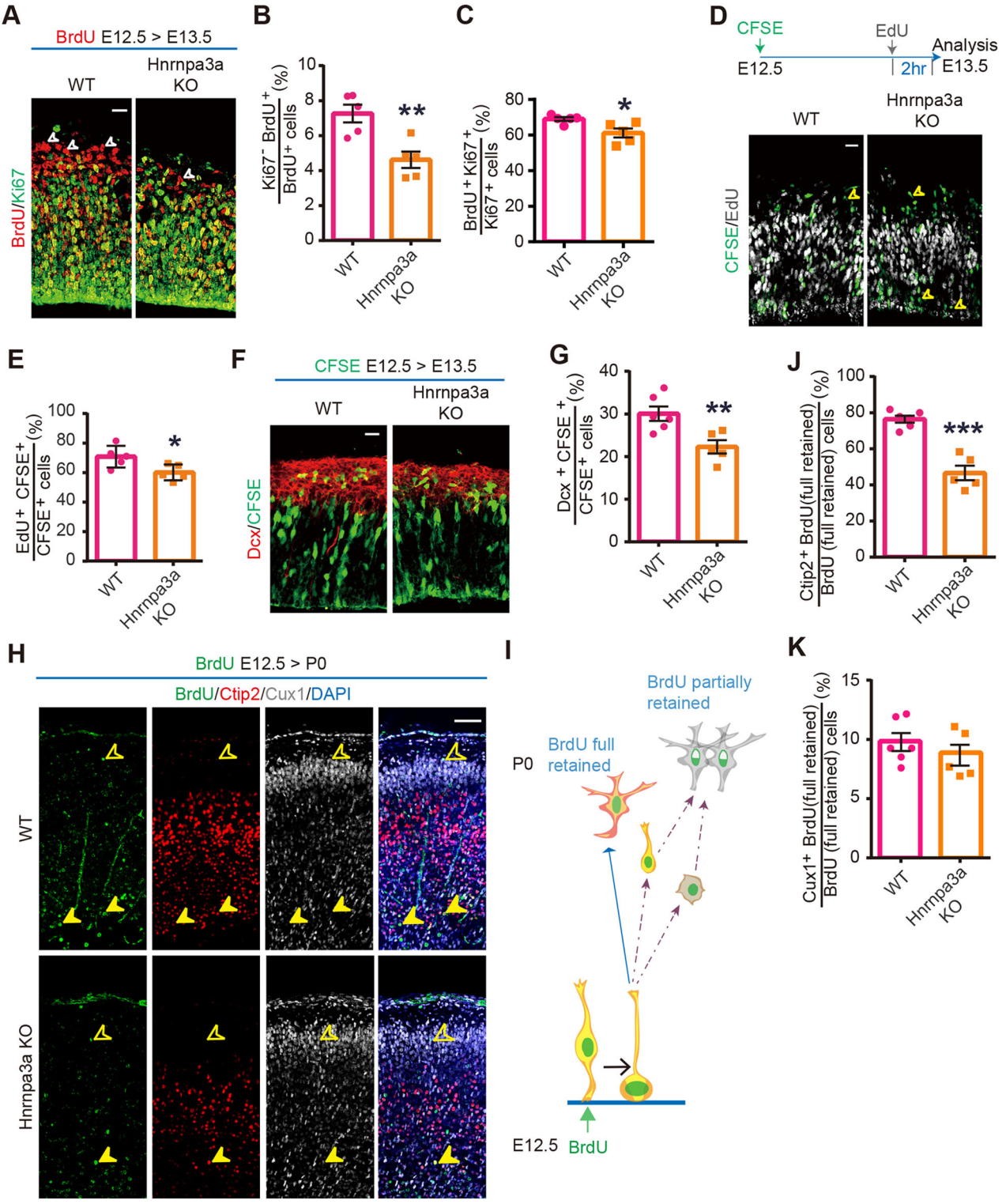

Fig. 7. Hnrnpa3a deletion impairs neurogenesis of early born deep-layer neurons. (A) E12.5 mice were subjected to pulse labeling with BrdU and examined 1 day later by staining with BrdU (red) and Ki67 (green). Arrowheads indicate $BrdU^{+}Ki67^{-}$ cells. Scale bar: 20 µm. (B,C) Quantification for the percentage of $BrdU^{+}Ki67^{-}$ cells among $BrdU^{+}$ cells (unpaired *t*-test, $^{**}P$=0.0052) (B) or $BrdU^{+}Ki67^{+}$ cells among $Ki67^{+}$ cells (Mann–Whitney test, $^{*}P$=0.0317) (C). At least five embryos were analyzed in each group. (D) E12.5 mice were pulse labeled with carboxy-fluorescein esters (CFSE) (green), followed by EdU (gray) labeling 1 day later and examined 2 h later. Arrowheads indicate $CFSE^{+}$ EdU^{-} cells. Scale bar: 20 µm. (E) Quantification of the percentage of $EdU^{+}CFSE^{+}$ cells among $CFSE^{+}$ cells (unpaired *t*-test, $^{*}P$=0.0497). (F) E12.5 mice were pulse labeled by CFSE and examined at E13.5 by staining with young neuronal marker Dcx. Scale bar: 20 µm. (G) Quantification of the percentage of $CFSE^{+}Dcx^{+}$ cells among $CFSE^{+}$ cells (unpaired *t*-test, $^{**}P$=0.009). At least five embryos were analyzed in each group. (H) E12.5 mice were subjected to pulse labeling with BrdU and analyzed at P0 by immunostaining for neuronal markers Ctip2 (red) and Cux1 (gray). Solid arrowheads indicate $Ctip2^{+}$ cells with fully retained BrdU; hollow arrowheads indicate $Cux1^{+}$ cells with fully retained BrdU. Scale bar: 50 µm. (I) Schematic of experiment in H. (J,K) Quantification of the percentage of $Ctip2^{+}$ or $Cux1^{+}$ cells among cells with fully retained BrdU: $^{***}P$<0.0001 (J); *P*=0.4359 (K); unpaired *t*-test. At least five embryos were analyzed in each group.

Development (2020) 147, dev185132. doi:10.1242/dev.185132

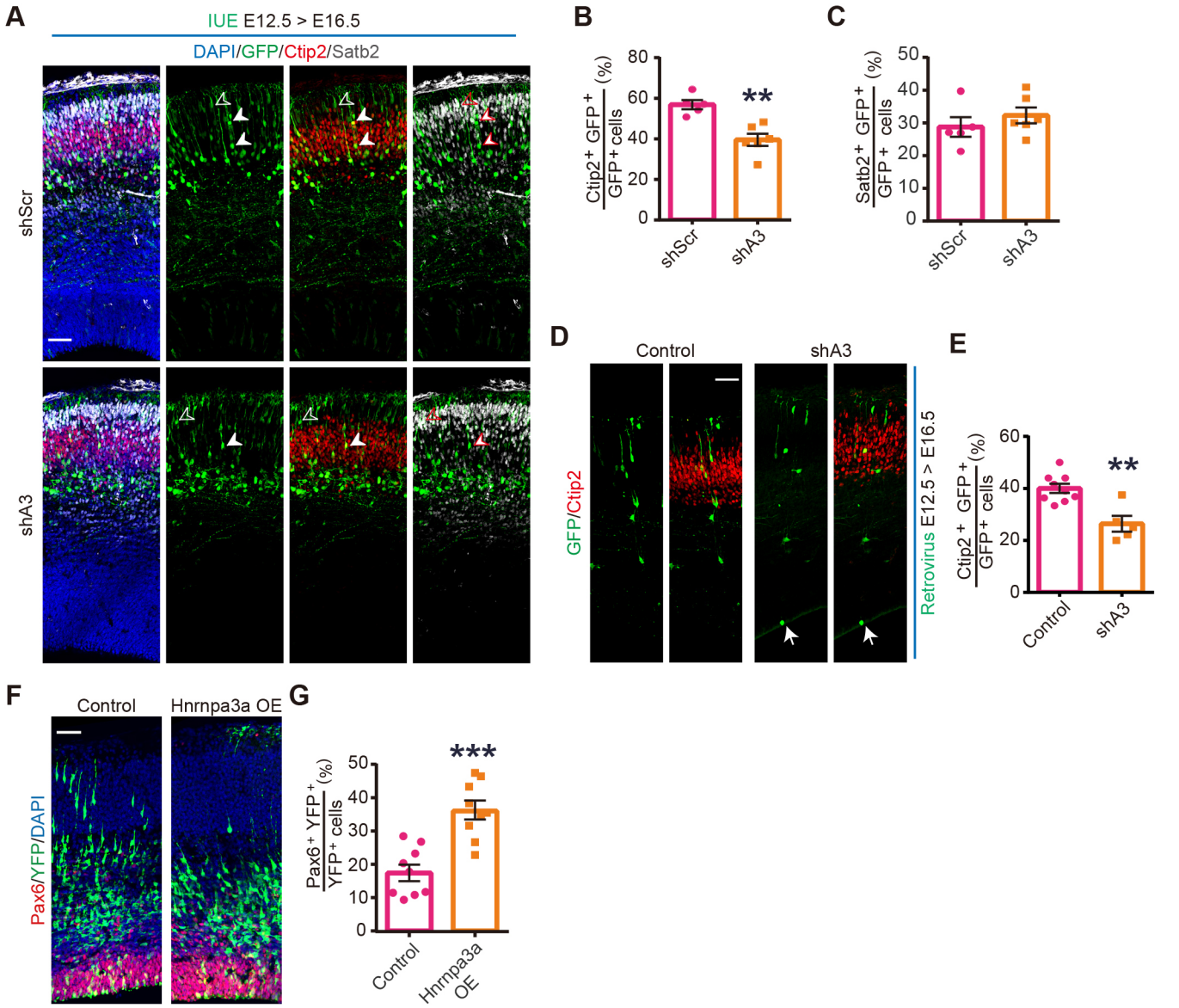

Fig. 8. Hnrnpa3a acts cell-autonomously on the neurogenesis of early born neurons in mice. (A) E12.5 mice were subjected to *in utero* electroporation with constructs encoding shA3 or shScr, and analyzed at E16.5 by immunostaining using antibodies against Ctip2 and Satb2. Solid arrowheads indicate Ctip2$^+$ GFP$^+$ cells. Hollow arrowheads indicate Satb2$^+$ GFP$^+$ cells. Scale bar: 50 µm. (B,C) Quantification of the percentage of Ctip2$^+$GFP$^+$ cells (B) or Satb2$^+$GFP$^+$ cells (C) among GFP$^+$ cells. Each dot in the diagram represents the value from one embryo. Unpaired *t*-test; ***P*=0.0016 (B), *P*=0.3777 (C). (D) Low titer of control or shA3-expressiong retrovirus was injected into telencephalic ventricles of E12.5 mice, followed by analysis at E16.5 by immunostaining for Ctip2 for progeny of resolvable clones distributed along vertical columns. Scale bar: 50 µm. (E) Quantification of the percentage of Ctip2$^+$ cells among GFP$^+$ retrovirus-infected cells (unpaired *t*-test, ***P*=0.0013). (F) E14.5 mouse cortex was subjected to IUE with vehicle control (pCAGGS) plasmid or plasmid expressing Hnrnpa3a (Hnrnpa3a OE), followed by YFP (green) and Pax6 (red) immunostaining at E16.5. Scale bar: 50 µm. (G) Quantification of the percentage of Pax6$^+$ cells among electroporated YFP-labeled cells (unpaired *t*-test with Welch's correction, ****P*<0.0001).

HOPX, which has been shown to be enriched in oRGs (Pollen et al., 2015). As shown in Fig. 9G, HOPX$^+$ cells were largely reduced in *HNRNPA3* knockdown organoids. This might be due to delayed switch from vRG to oRG or to direct effects on oRG proliferation. The effects of *HRNRPA3* downregulation on the pool of NPs were also reflected from reduced expression of a set of genes, which encode proteins either as markers or regulators of proliferative NPs involved in human cortex expansion (Fig. S7F). The activity of DNA damage or repair pathway displayed by γH2AX or phosphorylated ATM (pS1981) was also higher in *HNRNPA3* knockdown organoids (Fig. S7G-I). In summary, these results suggest that HNRNPA3 plays a crucial role in human cortex development.

DISCUSSION

In this study we present direct *in vivo* evidence supporting the conclusion that HNRNPA3 plays an important role in early neurogenesis in cortex development. We found that HNRNPA3 is enriched in cortical NPs with higher proliferation potency, including RGs in both mouse and human, as well as BPs in human, at early cortical developmental stages. The loss or knockdown of *Hnrnpa3a* resulted in mitotic delay in NPs and impaired cortical neurogenesis (see Fig. 9H for a proposed model). Interestingly, the defects in mice were more pronounced in early-born deep layer neurons than in late-born superficial layer neurons. The temporal dynamic expression pattern of Hnrnpa3 may underlie

Development (2020) 147, dev185132. doi:10.1242/dev.185132

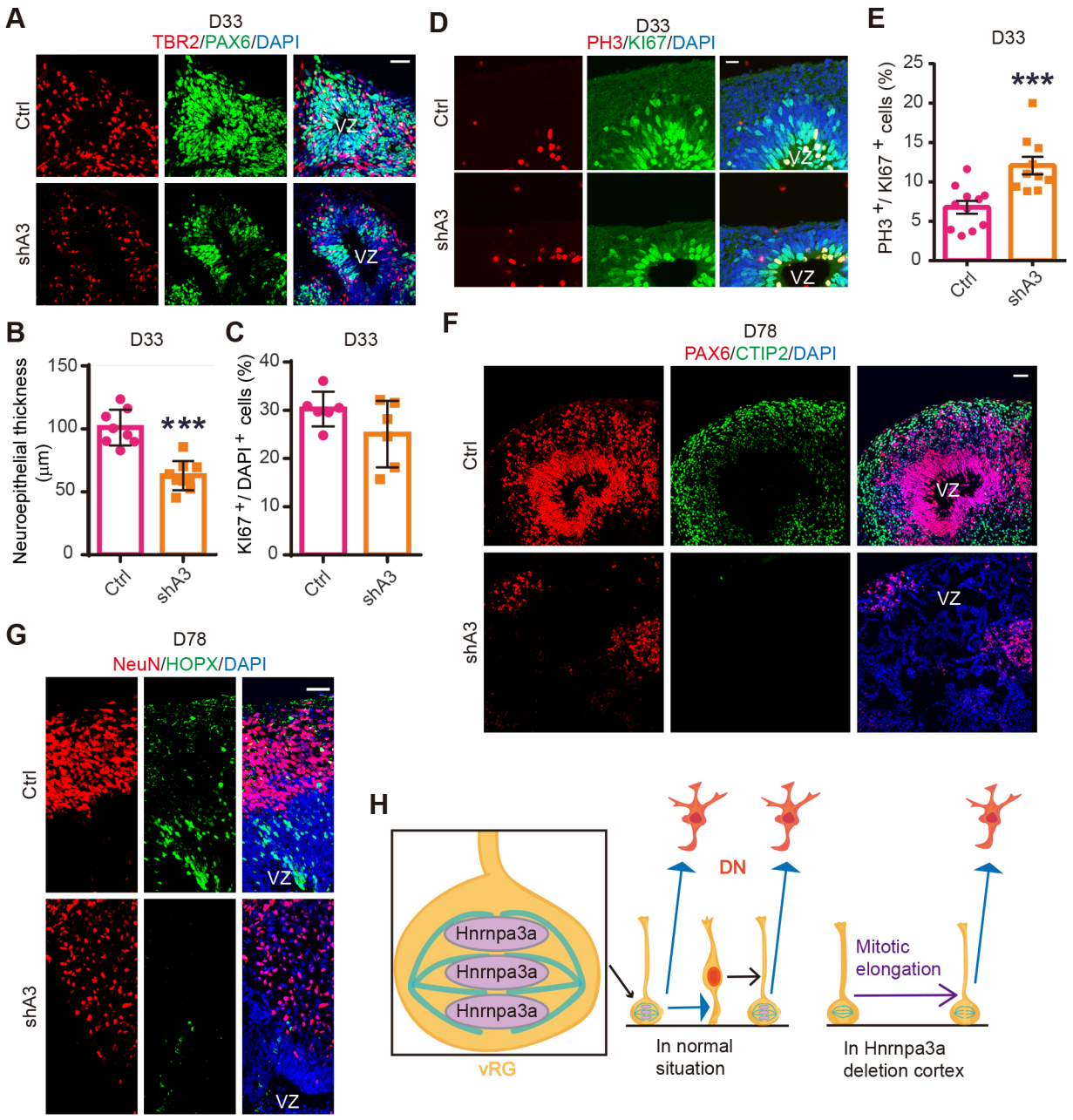

Fig. 9. Effects of *HNRNPA3* downregulation on human cerebral organoids. (A) Slices of control (Ctrl) or *HNRNPA3* knockdown (shA3) cerebral organoids at day 33 (D33) were labeled for RG marker PAX6 (green) and IP marker TBR2 (red). Scale bar: 50 µm. (B) Quantification for the neuroepithelial thickness of indicated organoids at day 33 (unpaired *t*-test, ***P<0.0001). Each dot in the graph represents the value of one organoid. (C) Quantification for the percentage of KI67$^+$ cells in indicated organoids (unpaired *t*-test, P=0.132). (D) Slices of organoids at day 33 were stained with KI67 (green) and PH3 (red). Scale bar: 20 µm. (E) Quantification of the ratio of PH3$^+$/KI67$^+$ cells in day 33 organoids (unpaired *t*-test, ***P=0.0009). (F,G) Slices of organoids at D78 were stained for PAX6 (red) and CTIP2 (green) (F) or for NeuN (red) and HOPX (green) (G). Scale bars: 50 µm. (H) Schematic representation for the role of Hnrnpa3 in direct neurogenesis of deep-layer neurons (DN). In the early period of cortical development, Hnrnpa3a is expressed at high levels in proliferative NPs, such as vRGs in mice, and distributed in peri-chromosome region. This pattern permits progression of division of early NPs, which give rise to early born deep-layer neurons via direct neurogenesis. Loss of Hnrnpa3a impairs chromosome segregation, leading to mitotic delay and reduction in the production of neuronal progeny.

its specific role, or alternatively, highly proliferative NPs might be more vulnerable to the loss of Hnrnpa3.

It is known that excitatory cortical neurons form six layers, with deep layer neurons (layers VI and V) born early and superficial layer neurons (layers II-IV) born later, and the successive process extends days in the mouse (E10.5-E18.5) to months in humans (Jabaudon, 2017; Marin-Padilla, 1978; Silbereis et al., 2016). During early corticogenesis periods (E11.5-E13.5 in mice), RGs in the VZ can either self-amplify or differentiate into early born deep-layer neurons and this direct neurogenesis gradually decreases as cortical development proceeds (Jabaudon, 2017). At later stages (about E14.5-E16.5 in mice), indirect neurogenesis via IPs in the SVZ dominate to generate superficial layer neurons. Interestingly, the loss of *Hnrnpa3a* mainly exhibited defects in deep layers, rather than superficial layers. Given that loss or downregulation of *Hnrnpa3a* caused mitotic delay in RGs at the mouse VZ, we predict

Development (2020) 147, dev185132. doi:10.1242/dev.185132

that neurogenesis of early born neurons might be more vulnerable to the loss of *Hnrnpa3a* in NPs. Indeed, it has been hypothesized that fates of various types of cortical neurons might be predetermined by fate-restricted progenitors (Franco et al., 2012). This opinion was revised in a recent study that the fates of superficial layer neurons are affected by environmental signals rather than intrinsic transcriptional programming (Telley et al., 2019). In line with this notion, we did not observe changes in superficial layer neurons. This result is different from a recent study, which showed ectopic and increased neuronal fate specification under a condition with mitotic delay of NPs (Pilaz et al., 2016). This discrepancy might be due to either difference in temporal expression patterns or distinct functions in cell cycle phases. Indeed, it has been suggested that the neuronal fate might be pre-determined in NPs at G1 phase (Arai et al., 2011). Our results suggest that mitotic delay caused by Hnrnpa3a deficiency influences the replenishment of NPs and impairs neuronal competency.

HNRNPA3 was initially identified as a RNA-binding protein with a role in cytoplasmic trafficking of RNA (Ma et al., 2002). It has been reported that HNRNPA3 binds to hexanucleotide repeat (G4C2) RNA of the gene *C9orf72*, which is believed to be the most common cause of familial amyotrophic lateral sclerosis (ALS) or frontotemporal lobar degeneration (FTLD), and downregulation of HNRNPA3 increased the repeat RNA level and reproduced some features of *C9orf72* pathology in neurons (Mori et al., 2013, 2016). Other studies suggest that it binds to telomeric DNA sequence and protects it from nuclease attack *in vitro* (Huang et al., 2010; Tanaka et al., 2007). Here, we found that HNRNPA3 is distributed in peri-chromosome regions of mitotic NPs (Fig. 5A and Fig. S4A). This localization appears to be dependent on the integrity of microtubules, because microtubule depolymerization disrupted its association with chromosome (Fig. S4A). Notably, loss or downregulation of HNRNPA3 affected normal separation of sister chromatids with the appearance of chromatin bridges in NPs at anaphase, leading to mitotic delay (Fig. 5B,D and Fig. 4A). These effects were most likely due to HNRNPA3 regulation of cohesion complex (Fig. 6). Furthermore, HNRNPA3 has been shown to be associated with telomeres directly (Tanaka et al., 2007). This association might protect integrity of chromosomes during NP division. It has been suggested that early neurogenesis from vRG is more vulnerable to chromosome defects (Lee et al., 2012a,b; Vargas-Hurtado et al., 2019). Considering the role of HNRNP family proteins in regulating alternative RNA splicing (Cáceres and Kornblihtt, 2002; Han et al., 2010), it remains possible that products of impaired alternative splicing may underlie the phenotypes caused by the loss of *HNRNPA3*. Indeed, evolutionarily or cell type specific alternative splicing has been shown to regulate cortex development (Bae et al., 2014; Zhang et al., 2016).

In humans and other non-human primates, the remarkable expansion of cortical surface is believed to attribute to increased proliferative capacity of NPs (Dehay et al., 2015). Unlike rodents, both apical and basal NPs in primates display high proliferation potency and exhibit similar gene expression patterns (Florio et al., 2015). In cultured human cerebral organoids, downregulation of *HNRNPA3* markedly reduced both apical and basal progenitors (Fig. 9A), in line with the observation that *HNRNPA3* is highly expressed in human VZ and oSVZ (Fig. 1B), two major regions containing heterogeneous types of proliferative NPs. It appears that the effects on human cortical development are more severe than on mice. One probable reason is that human corticogenesis requires more rounds of NP divisions to meet the need for lateral and vertical expansion, and the mitotic delay caused by downregulation of *HNRNPA3* impaired the NP pool size.

Collectively, these results indicate that the role of HNRNPA3 is conserved in mammals and suggest that the NPs with higher proliferative potency are more vulnerable to retardation in cell cycle progression. Considering that defects in NP divisions are major causes of microcephaly, it would be of interest to link *HNRNPA3* mutations, if any, with MCPH or other mental retardation diseases. It would also be interesting to check whether *HNRNPA3* deletion contributes to mental retardation in individuals with deletion in 2q3.2 (OMIM #612345), where *HNRNPA3* gene is located (Mencarelli et al., 2007).

MATERIALS AND METHODS

Fetal brain samples

Human fetal brain samples were obtained after medical pregnancy termination with informed consent, following standard procedure and institutional ethic guidelines in hospital, and with approval of the Shanghai Institutes for Biological Sciences Ethical Committee, Chinese Academy of Sciences (Approval Identifier Number: ER-SIBS-221506). Gestational age was checked by ultrasonic measurements. Fetal brain samples were temporarily preserved in ice-cold Leibowitz-15 medium (Gibco, 21083027) before further laboratory procedures.

Mice

The *Hnrnpa3* knockout (KO) mice in the *C57BL/6* background (MGI: 5812384) were generated with CRISPR/Cas9 technology as submission record (MGI Ref. ID: J:237332). The zygotes at the two-cell stage were transferred into oviducts of pseudo-pregnant females. Newborns were further bred in accordance with standard procedures and animal welfare. The genotype of offspring from heterogeneous crossings was determined by PCR with LA Taq (Takara, RR02AG). The sequences of primers were: 5′-GGATAGCACATCACGTGGTGACTGG-3′ (forward, F) and 5′-GCTAAGTCAGGCCGCGCAGC-3′ (reverse, R). The C57BL/6 pregnant mice were used for *in utero* electroporation experiments. All animal experiments abided by the guidelines of the Institutional Animal Care and Use Committee of the Institute of Neuroscience, Chinese Academy of Sciences and ShanghaiTech University.

Plasmids and virus preparation

To mark Hnrnpa3 localization, the *Hnrnpa3*-coding sequence (NM_198090) fused with *EYFP* sequence at the C terminus was cloned into the pCAG vector using *ASCI* and *AgeI* restriction enzymes (New England Biolabs). For overexpression experiments, the *Hnrnpa3*-coding sequence was cloned into the pCAGGS-EGFP plasmid. As the translation product of human *HNRNPA3* is almost identical to that of *Hnrnpa3a* in mice, the mouse *Hnrnpa3* construct was introduced into human cells for the analysis of subcellular localization. The shRNA targeting against conserved sequence between mouse and human *HNRNPA3* (5′-AGAGAGCTGTTT-CTAGAGA-3′) (Huang et al., 2010) or scrambled sequence (5′-GGTGA-GCTATGTACGTAAA-3′) was cloned into pSUPER vector for *in utero* electroporation experiments, and cloned into the lentivirus vector pTRIPZ, which harbors puromycin resistance, a doxycycline-inducible tetracycline turn-on element and RFP reporter gene, for the infection of H9 human embryonic stem cells.

Cell culture and transfection

Human neural progenitor ReNeuron (ReN) cells were maintained on 15-40 µg/ml laminin (Sigma-Aldrich, L2020-1MG)-coated dishes in the medium containing 2% B27 without VA (Gibco, 12587010), 10 units/ml heparin (Sigma-Aldrich, H3149-100KU), 20 ng/ml EGF (Millipore, GF155) and 10 ng/ml bFGF (STEMCELL, 78003) in DMEM/F12 (Gibco, 11330057). After forced expression of HNRNPA3 in ReN cells, culture medium was replaced with differentiation medium [0.5×N2 supplement, 0.5×B27 supplement (Gibco, 17504044), in 50% DMEM/F12, 50% Neurobasal (Gibco, 12348017)]. ReN cells were transfected with

Development (2020) 147, dev185132. doi:10.1242/dev.185132

Lipofectamine 3000 Transfection Reagent (Invitrogen, L3000015). ReN cells were treated with nocodazole (Sigma, M1404-2MG) (100 ng/ml) for 6 h to induce microtubule de-polymerization.

RNA extraction and qPCR analysis

Total RNA extracted from two or three organoids were isolated with RNeasy Plus Micro Kit (Qiagen, Germany, 74034). For reverse transcription, 2 µl total mRNA was processed with GoScript Reverse Transcription Kit (Promega, A5001). Quantitative PCR using SYBR Green PCR mix (Biotool, B21702) was performed on Roche LightCycler with primers listed in Table S1. For each transcript, raw values were normalized with that of GAPDH.

Human ES cell and brain organoid culture

H9 human embryonic stem (hES) cells were infected by lentivirus with pTRIPZ vector encoding siRNA against *HNRNPA3* or control sequence and cultured for 3 days on Matrigel (Corning, 354277)-coated dishes in mTeSR1 medium (STEMCELL, 5850), followed by addition of puromycin (1 µg/ml) for 4 days to select infected clones. After at least two rounds of selection, active proliferative clones were digested with enzyme-free passage reagent ReLeSR (STEMCELL, 05872), passaged in a 1:10-1:40 ratio and cultured in puromycin-containing mTeSR1. Then, hES clones were digested with Accutase (Sigma-Aldrich, A6964-100ML) to generate a single cell suspension, followed by incubation with mTeSR1 containing 10 µM Y27632 to allow embryonic body (EB) formation. Around 7000 cells were seeded into each well of V-bottom 96-well plate (NUNC, 277143) coated with lipidure (Nof, CM5206). The time point of EB induction was designated as day 0. After 2-3 days, the culture medium was replaced with the medium containing 20% Knockout Serum Replacer (Gibco, 10828028), 1×MEM-NEAA (Gibco, 11140050), 3.5 µl/l β-mercaptoethanol (Sigma-Aldrich, M3148), 1×Glutamax (Gibco, 35050061), 2.5 µM dorsomorphine (Tocris, 3093/10) and 2 µM A83-01 (Tocris, 2939/10), in DMEM/F12 for ectodermal induction. After another 4 days, EBs were placed in neural induction medium containing 1×N2 Supplement (Gibco, 17502048), 1×Glutamax (Gibco), 1×MEM-NEAA (Gibco) and 1 µg/ml heparin in DMEM/F12 with half the medium renewed every other day. To turn on the siRNA expression, 1 µg/ml doxycycline was added into the medium from the second day of neural induction. After 6 days of neural induction, the neuroepithelial organoids were embedded into growth factor-reduced Matrigel droplet, as described previously (Lancaster and Knoblich, 2014), and fed with differentiation medium [0.5×N2 supplement, 0.5×B27 supplement without vitamin A, 3.5 µl/l β-mercaptoethanol, 250 µl/l Insulin (Sigma-Aldrich, I9278), 1×Glutamax and 0.5×MEM-NEAA, 1×Antibiotic-Antimycotic (Gibco, 15240096), in 50% DMEM/F12 and 50% Neurobasal medium)], with medium renewed every other day. After 4 days in differentiation medium, the organoids were transferred into maturation medium [0.5×N2 supplement, 0.5×B27 supplement (Gibco, 17504044), 3.5 µl/l β-mercaptoethanol, 250 µl/l insulin, 1×Glutamax and 0.5×MEM-NEAA, and 1×Antibiotic-Antimycotic, in 50% DMEM/F12, 50% Neurobasal medium] and then placed on a shaker in a 5% CO_2 incubator and cultured at 37°C for different days with medium renewal every 2-3 days.

Clone analysis

Control or shA3-expressing retrovirus (1 µl, ∼$1×10^7$ TU/ml) was injected into the telencephalic ventricles of E12.5 mice. Four days later, embryonic brains were fixed, dehydrated and cryostat-sectioned at 35 µm, followed by immunostaining. GFP^+ cells aligned along a single vertical trajectory from apical to basal axis were considered as the progeny of a neural progenitor.

In utero electroporation

Pregnant mice at different gestation days were anesthetized with pentobarbital sodium, then plasmids (2 µg/µl) mixed with 0.25% Fast Green (Sigma-Aldrich) in sterile PBS were gently injected into the telencephalic ventricles of each embryos using a glass micropipette (VWR International). Immediately after injection, embryonic brains were subjected to electroporation at given pulses (28 V, 5×50 ms pulses with 1 s interval) with two 3 mm (in radius) disc electrodes (BEX, Japan, LF650P3) using an electroporator (BTX, ECM830).

Cell-cycle kinetics analysis

To label NPs at S-phase, the pregnant female mouse was injected intraperitoneally with BrdU (Sigma-Aldrich) at 50 mg/kg. To trace mitotic progenitors, 1 µl CellTrace reagent carboxy-fluorescein esters (shorted as CFSE) (Invitrogen, C34554) was injected into the telencephalic vehicle of E12.5 mice; 22 h later, pregnant mice were subjected to intraperitoneal EdU (100 µg) injection. At E13.5, brain slices were stained with antibodies against EdU or Dcx to measure cell cycle re-entry or neuronal differentiation. To measure mitotic index, embryos were fixed 6 h after EdU pulse at E12.5. To label proliferative ReN cells, EdU (10 µM) was added into differentiation medium and cultured for an additional 2 h. The immunofluorescence signals of BrdU and EdU were measured following the manufacturer's protocol (Abcam).

Histological analysis, immunostaining, immunoprecipitation and immunoblotting

Tissues from mice and organoids were fixed with 4% PFA in 1×PBS at 4°C overnight, followed by dehydration with 20-30% sucrose in PBS. Tissues were then embedded in OCT and cryosectioned at 20-40 µm thickness. Lung sections were stained with Hematoxylin and Eosin (HE) for morphological analysis. To optimize the immunofluorescence signals, sections were incubated in antigen retrieval solution (Beyotime Biotechnology, P0090) for 20-60 min at room temperature and washed three times with PBS, followed by incubation in 0.3% Triton X-100 for around 30 min. To avoid background staining, sections were blocked with 5% BSA in PBS at room temperature for 1 h or at 4°C for more than 2 h. Slices were incubated with primary antibodies in blocking solution overnight at 4°C; after extensive washes, they were incubated with secondary antibodies for about 24 h at 4°C. For immunofluorescence observation of cultured cells, the fixation was shortened to 15 min at room temperature and permeabilization was adjusted to 0.25% Triton X-100 for about 10 min. For organoid sections, the incubation of primary antibodies was prolonged to 2 days. HNRNPA3 antibody was conjugated with Cy3 using Fast Conjugation Kit (Abcam, ab188287). For immunoprecipitation, 30 µl protein A/G magnetic beads (Bimake, B23201) were washed with RIPA buffer and incubated with antibody against SMC1A or IgG at 4°C overnight followed by three washes using RIPA buffer to clear unbound antibody, and then incubated with cell lysates with rotation overnight at 4°C. After three RIPA washes, bound proteins were eluted from beads by boiling with 1× loading buffer for 10 min.

For immunoblotting, adherent cells were harvested using 0.05% Trypsin and washed several times with ice-cold PBS. Cell pellets collected by centrifugation were lysed in RIPA buffer [50 mM Tris-HCl (pH 7.4), 150 mM NaCl, 1% NP-40, 0.5% sodium deoxycholate] containing Protease Inhibitor Cocktail Set III (Millipore, 539134-1SETCN) for 20 min on ice. Further protein solutions were prepared by centrifugation at 16,000 ***g*** for 15 min at 4°C and boiled with 5×SDS sample buffer for 5 min at 95°C. For tissue samples, we used mechanical cutting and RIPA treatment for a longer time to enhance the lysis. For immunoblotting, lysates were loaded in 12% SDS-PAGE and then transferred onto 0.45 µm PVDF membranes at 100 V. Subsequently, PVDF membranes were blocked in 5% BSA in TBS-T for 1 h at room temperature, then incubated with primary antibodies diluted in 3% BSA/TBS-T at 4°C for more than 16 h, followed by three washes in TBS-T and incubation with HRP-conjugated secondary antibodies diluted in 3% BSA/TBST at room temperature for 2 h or 4°C overnight. Finally, blots were washed several times in TBS-T and imaged using a Tanon 4600 Chemiluminescent Imaging System. The primary antibodies used are listed in Table S2.

Time-lapse imaging

Live imaging of cortical slice was performed as described previously (Pilaz and Silver, 2014) with minor modifications. Briefly, embryonic brains were sectioned at 250 µm using a Leica VT1200S vibratome. After Hoechst (ThermoFisher, H3570) staining for 8 min, slices were mounted on glass-bottomed dishes (WPI) with Matrigel. Slices were cultured in slice culture medium (Pilaz and Silver, 2014) containing ProLong Live Antifade Reagent (ThermoFisher, P36975). Live imaging was performed at 37°C in 5% CO_2 on FV10 microscope (Olympus).

Quantification and statistical analysis

For phenotypic analysis, *Hnrnpa3* KO mice and their wild-type littermates from at least three mothers were analyzed. For *in utero* electroporation and virus injection experiments, each experiment was performed in three or four pregnant mice in each group. The results were obtained from slices at the same lateral-medial level and the rostral-caudal axis and all images were processed with Fiji software. Raw digital data were analyzed by Graphpad Prism 6 and results are presented as mean±s.e.m. Quantitative differences were determined using the Kolmogorov–Smirnov test, an unpaired *t*-test, an unpaired *t*-test with Welch's correction or a Mann–Whitney test. The statistical significance was indicated as: *P<0.05; **P<0.01; ***P<0.001. All tests were two-tailed.

Competing interests

The authors declare no competing or financial interests.

Author contributions

Conceptualization: Z.-G.L.; Methodology: M.-Y.O., X.-C.J., Y.-J.C., X.-Y.S.; Validation: M.-Y.O., J.-F.W.; Formal analysis: M.-Y.O., X.-C.J.; Investigation: M.-Y.O., Y.-J.C., X.-Y.S., J.-F.W., X.-Q.F., Q.S.; Resources: Q.S., Z.-G.L.; Data curation: M.-Y.O., X.-C.J., J.-F.W., X.-Q.F.; Writing - original draft: M.-Y.O., Z.-G.L.; Writing - review & editing: Z.-G.L.; Supervision: Z.-G.L.; Project administration: Z.-G.L.; Funding acquisition: Z.-G.L.

Funding

This study was partially supported by grants from the National Natural Science Foundation of China (31490591 to Z.-G.L. and 31871034 to X.-C.J.), the National Key R&D Program of China (2017YFA0700500), the Frontier Key Project of the Chinese Academy of Sciences (QYZDJ-SSW-SMC025), the Shanghai Municipal Science and Technology Major Project (2018SHZDZX05) and the start-up support of ShanghaiTech University.

Supplementary information

Supplementary information available online at
http://dev.biologists.org/lookup/doi/10.1242/dev.185132.supplemental

Peer review history

The peer review history is available online at https://dev.biologists.org/lookup/doi/10.1242/dev.185132.reviewer-comments.pdf

References

Angevine, J. B. and Sidman, R. L. (1961). Autoradiographic study of cell migration during histogenesis of cerebral cortex in the mouse. *Nature* **192**, 766-768. doi:10.1038/192766b0

Arai, Y., Pulvers, J. N., Haffner, C., Schilling, B., Nüsslein, I., Calegari, F. and Huttner, W. B. (2011). Neural stem and progenitor cells shorten S-phase on commitment to neuron production. *Nat. Commun.* **2**, 154. doi:10.1038/ncomms1155

Bae, B.-I., Tietjen, I., Atabay, K. D., Evrony, G. D., Johnson, M. B., Asare, E., Wang, P. P., Murayama, A. Y., Im, K., Lisgo, S. N. et al. (2014). Evolutionarily dynamic alternative splicing of GPR56 regulates regional cerebral cortical patterning. *Science* **343**, 764-768. doi:10.1126/science.1244392

Barrera, J. A., Kao, L.-R., Hammer, R. E., Seemann, J., Fuchs, J. L. and Megraw, T. L. (2010). CDK5RAP2 regulates centriole engagement and cohesion in mice. *Dev. Cell* **18**, 913-926. doi:10.1016/j.devcel.2010.05.017

Betizeau, M., Cortay, V., Patti, D., Pfister, S., Gautier, E., Bellemin-Ménard, A., Afanassieff, M., Huissoud, C., Douglas, R. J., Kennedy, H. et al. (2013). Precursor diversity and complexity of lineage relationships in the outer subventricular zone of the primate. *Neuron* **80**, 442-457. doi:10.1016/j.neuron.2013.09.032

Cáceres, J. F. and Kornblihtt, A. R. (2002). Alternative splicing: multiple control mechanisms and involvement in human disease. *Trends Genet.* **18**, 186-193. doi:10.1016/S0168-9525(01)02626-9

Camp, J. G., Badsha, F., Florio, M., Kanton, S., Gerber, T., Wilsch-Bräuninger, M., Lewitus, E., Sykes, A., Hevers, W., Lancaster, M. et al. (2015). Human cerebral organoids recapitulate gene expression programs of fetal neocortex development. *Proc. Natl. Acad. Sci. USA* **112**, 15672-15677. doi:10.1073/pnas.1520760112

Cárdenas, A., Villalba, A., de Juan Romero, C., Picó, E., Kyrousi, C., Tzika, A. C., Tessier-Lavigne, M., Ma, L., Drukker, M., Cappello, S. et al. (2018). Evolution of cortical neurogenesis in amniotes controlled by robo signaling levels. *Cell* **174**, 590-606.e521. doi:10.1016/j.cell.2018.06.007

Chenn, A. and Walsh, C. A. (2002). Regulation of cerebral cortical size by control of cell cycle exit in neural precursors. *Science* **297**, 365-369. doi:10.1126/science.1074192

Crasta, K., Ganem, N. J., Dagher, R., Lantermann, A. B., Ivanova, E. V., Pan, Y., Nezi, L., Protopopov, A., Chowdhury, D. and Pellman, D. (2012). DNA breaks and chromosome pulverization from errors in mitosis. *Nature* **482**, 53-58. doi:10.1038/nature10802

Dehay, C., Kennedy, H. and Kosik, K. S. (2015). The outer subventricular zone and primate-specific cortical complexification. *Neuron* **85**, 683-694. doi:10.1016/j.neuron.2014.12.060

Dreyfuss, G., Matunis, M. J., Pinol-Roma, S. and Burd, C. G. (1993). hnRNP proteins and the biogenesis of mRNA. *Annu. Rev. Biochem.* **62**, 289-321. doi:10.1146/annurev.bi.62.070193.001445

Fietz, S. A., Kelava, I., Vogt, J., Wilsch-Bräuninger, M., Stenzel, D., Fish, J. L., Corbeil, D., Riehn, A., Distler, W., Nitsch, R. et al. (2010). OSVZ progenitors of human and ferret neocortex are epithelial-like and expand by integrin signaling. *Nat. Neurosci.* **13**, 690-699. doi:10.1038/nn.2553

Florio, M. and Huttner, W. B. (2014). Neural progenitors, neurogenesis and the evolution of the neocortex. *Development* **141**, 2182-2194. doi:10.1242/dev.090571

Florio, M., Albert, M., Taverna, E., Namba, T., Brandl, H., Lewitus, E., Haffner, C., Sykes, A., Wong, F. K., Peters, J. et al. (2015). Human-specific gene ARHGAP11B promotes basal progenitor amplification and neocortex expansion. *Science* **347**, 1465-1470. doi:10.1126/science.aaa1975

Franco, S. J., Gil-Sanz, C., Martinez-Garay, I., Espinosa, A., Harkins-Perry, S. R., Ramos, C. and Müller, U. (2012). Fate-restricted neural progenitors in the mammalian cerebral cortex. *Science* **337**, 746-749. doi:10.1126/science.1223616

Gruber, R., Zhou, Z., Sukchev, M., Joerss, T., Frappart, P.-O. and Wang, Z.-Q. (2011). MCPH1 regulates the neuroprogenitor division mode by coupling the centrosomal cycle with mitotic entry through the Chk1-Cdc25 pathway. *Nat. Cell Biol.* **13**, 1325-1334. doi:10.1038/ncb2342

Guan, J., Ekwurtzel, E., Kvist, U. and Yuan, L. (2008). Cohesin protein SMC1 is a centrosomal protein. *Biochem Biophys Res. Commun.* **372**, 761-764. doi:10.1016/j.bbrc.2008.05.120

Haarhuis, J. H. I., Elbatsh, A. M. O. and Rowland, B. D. (2014). Cohesin and its regulation: on the logic of X-shaped chromosomes. *Dev. Cell* **31**, 7-18. doi:10.1016/j.devcel.2014.09.010

Han, S. P., Tang, Y. H. and Smith, R. (2010). Functional diversity of the hnRNPs: past, present and perspectives. *Biochem. J.* **430**, 379-392. doi:10.1042/BJ20100396

Hansen, D. V., Lui, J. H., Parker, P. R. L. and Kriegstein, A. R. (2010). Neurogenic radial glia in the outer subventricular zone of human neocortex. *Nature* **464**, 554-561. doi:10.1038/nature08845

Haubensak, W., Attardo, A., Denk, W. and Huttner, W. B. (2004). Neurons arise in the basal neuroepithelium of the early mammalian telencephalon: a major site of neurogenesis. *Proc. Natl. Acad. Sci. USA* **101**, 3196-3201. doi:10.1073/pnas.0308600100

Huang, P.-R., Hung, S.-C. and Wang, T.-C. V. (2010). Telomeric DNA-binding activities of heterogeneous nuclear ribonucleoprotein A3 in vitro and in vivo. *Biochim. Biophys. Acta* **1803**, 1164-1174. doi:10.1016/j.bbamcr.2010.06.003

Insolera, R., Bazzi, H., Shao, W., Anderson, K. V. and Shi, S.-H. (2014). Cortical neurogenesis in the absence of centrioles. *Nat. Neurosci.* **17**, 1528-1535. doi:10.1038/nn.3831

Jabaudon, D. (2017). Fate and freedom in developing neocortical circuits. *Nat. Commun.* **8**, 16042. doi:10.1038/ncomms16042

Jayaraman, D., Kodani, A., Gonzalez, D. M., Mancias, J. D., Mochida, G. H., Vagnoni, C., Johnson, J., Krogan, N., Harper, J. W., Reiter, J. F. et al. (2016). Microcephaly proteins Wdr62 and Aspm define a mother centriole complex regulating centriole biogenesis, apical complex, and cell fate. *Neuron* **92**, 813-828. doi:10.1016/j.neuron.2016.09.056

Ju, X.-C., Hou, Q.-Q., Sheng, A.-L., Wu, K.-Y., Zhou, Y., Jin, Y., Wen, T., Yang, Z., Wang, X. and Luo, Z.-G. (2016). The hominoid-specific gene TBC1D3 promotes generation of basal neural progenitors and induces cortical folding in mice. *eLife* **5**, e18197. doi:10.7554/eLife.18197

Kageyama, J., Wollny, D., Treutlein, B. and Camp, J. G. (2018). ShinyCortex: exploring single-cell transcriptome data from the developing human cortex. *Front. Neurosci.* **12**, 315. doi:10.3389/fnins.2018.00315

Kaindl, A. M., Passemard, S., Kumar, P., Kraemer, N., Issa, L., Zwirner, A., Gerard, B., Verloes, A., Mani, S. and Gressens, P. (2010). Many roads lead to primary autosomal recessive microcephaly. *Prog. Neurobiol.* **90**, 363-383. doi:10.1016/j.pneurobio.2009.11.002

Krecic, A. M. and Swanson, M. S. (1999). hnRNP complexes: composition, structure, and function. *Curr. Opin. Cell Biol.* **11**, 363-371. doi:10.1016/S0955-0674(99)80051-9

Lancaster, M. A. and Knoblich, J. A. (2014). Generation of cerebral organoids from human pluripotent stem cells. *Nat. Protoc.* **9**, 2329-2340. doi:10.1038/nprot.2014.158

Lange, C., Huttner, W. B. and Calegari, F. (2009). Cdk4/cyclinD1 overexpression in neural stem cells shortens G1, delays neurogenesis, and promotes the generation and expansion of basal progenitors. *Cell Stem Cell* **5**, 320-331. doi:10.1016/j.stem.2009.05.026

Lee, Y., Katyal, S., Downing, S. M., Zhao, J., Russell, H. R. and McKinnon, P. J. (2012a). Neurogenesis requires TopBP1 to prevent catastrophic replicative DNA damage in early progenitors. *Nat. Neurosci.* **15**, 819-826. doi:10.1038/nn.3097

Lee, Y., Shull, E. R. P., Frappart, P.-O., Katyal, S., Enriquez-Rios, V., Zhao, J., Russell, H. R., Brown, E. J. and McKinnon, P. J. (2012b). ATR maintains select progenitors during nervous system development. *EMBO J.* **31**, 1177-1189. doi:10.1038/emboj.2011.493

Li, Y., Muffat, J., Omer, A., Bosch, I., Lancaster, M. A., Sur, M., Gehrke, L., Knoblich, J. A. and Jaenisch, R. (2017). Induction of Expansion and Folding in Human Cerebral Organoids. *Cell Stem Cell* **20**, 385-396.e3. doi:10.1016/j.stem.2016.11.017

Lizarraga, S. B., Margossian, S. P., Harris, M. H., Campagna, D. R., Han, A. P., Blevins, S., Mudbhary, R., Barker, J. E., Walsh, C. A. and Fleming, M. D. (2010). Cdk5rap2 regulates centrosome function and chromosome segregation in neuronal progenitors. *Development* **137**, 1907-1917. doi:10.1242/dev.040410

Lui, J. H., Hansen, D. V. and Kriegstein, A. R. (2011). Development and evolution of the human neocortex. *Cell* **146**, 18-36. doi:10.1016/j.cell.2011.06.030

Ma, A. S. W., Moran-Jones, K., Shan, J., Munro, T. P., Snee, M. J., Hoek, K. S. and Smith, R. (2002). Heterogeneous nuclear ribonucleoprotein A3, a novel RNA trafficking response element-binding protein. *J. Biol. Chem.* **277**, 18010-18020. doi:10.1074/jbc.M200050200

Ma, Z., Lin, M., Li, K., Fu, Y., Liu, X., Yang, D., Zhao, Y., Zheng, J. and Sun, B. (2013). Knocking down SMC1A inhibits growth and leads to G2/M arrest in human glioma cells. *Int. J. Clin. Exp. Pathol.* **6**, 862-869.

Mairet-Coello, G., Tury, A., Van Buskirk, E., Robinson, K., Genestine, M. and DiCicco-Bloom, E. (2012). p57(KIP2) regulates radial glia and intermediate precursor cell cycle dynamics and lower layer neurogenesis in developing cerebral cortex. *Development* **139**, 475-487. doi:10.1242/dev.067314

Malatesta, P., Hartfuss, E. and Götz, M. (2000). Isolation of radial glial cells by fluorescent-activated cell sorting reveals a neuronal lineage. *Development* **127**, 5253-5263.

Marin-Padilla, M. (1978). Dual origin of the mammalian neocortex and evolution of the cortical plate. *Anat. Embryol.* **152**, 109-126. doi:10.1007/BF00315920

Mencarelli, M. A., Caselli, R., Pescucci, C., Hayek, G., Zappella, M., Renieri, A. and Mari, F. (2007). Clinical and molecular characterization of a patient with a 2q31.2-32.3 deletion identified by array-CGH. *Am. J. Med. Genet. A* **143A**, 858-865. doi:10.1002/ajmg.a.31602

Miller, J. A., Ding, S.-L., Sunkin, S. M., Smith, K. A., Ng, L., Szafer, A., Ebbert, A., Riley, Z. L., Royall, J. J., Aiona, K. et al. (2014). Transcriptional landscape of the prenatal human brain. *Nature* **508**, 199-206. doi:10.1038/nature13185

Miyata, T., Kawaguchi, A., Saito, K., Kawano, M., Muto, T. and Ogawa, M. (2004). Asymmetric production of surface-dividing and non-surface-dividing cortical progenitor cells. *Development* **131**, 3133-3145. doi:10.1242/dev.01173

Mora-Bermúdez, F. and Huttner, W. B. (2015). Novel insights into mammalian embryonic neural stem cell division: focus on microtubules. *Mol. Biol. Cell* **26**, 4302-4306. doi:10.1091/mbc.E15-03-0152

Mori, K., Lammich, S., Mackenzie, I. R. A., Forné, I., Zilow, S., Kretzschmar, H., Edbauer, D., Janssens, J., Kleinberger, G., Cruts, M. et al. (2013). hnRNP A3 binds to GGGGCC repeats and is a constituent of p62-positive/TDP43-negative inclusions in the hippocampus of patients with C9orf72 mutations. *Acta. Neuropathol.* **125**, 413-423. doi:10.1007/s00401-013-1088-7

Mori, K., Nihei, Y., Arzberger, T., Zhou, Q., Mackenzie, I. R., Hermann, A., Hanisch, F.; German Consortium for Frontotemporal Lobar Degeneration; Bavarian Brain Banking Alliance, Kamp, F. et al. (2016). Reduced hnRNPA3 increases C9orf72 repeat RNA levels and dipeptide-repeat protein deposition. *EMBO. Rep.* **17**, 1314-1325. doi:10.15252/embr.201541724

Nicholas, A. K., Khurshid, M., Désir, J., Carvalho, O. P., Cox, J. J., Thornton, G., Kausar, R., Ansar, M., Ahmad, W., Verloes, A. et al. (2010). WDR62 is associated with the spindle pole and is mutated in human microcephaly. *Nat. Genet.* **42**, 1010-1014. doi:10.1038/ng.682

Nishiyama, T., Sykora, M. M., Huis in 't Veld, P. J., Mechtler, K. and Peters, J.-M. (2013). Aurora B and Cdk1 mediate Wapl activation and release of acetylated cohesin from chromosomes by phosphorylating Sororin. *Proc. Natl. Acad. Sci. USA* **110**, 13404-13409. doi:10.1073/pnas.1305020110

Noctor, S. C., Flint, A. C., Weissman, T. A., Dammerman, R. S. and Kriegstein, A. R. (2001). Neurons derived from radial glial cells establish radial units in neocortex. *Nature* **409**, 714-720. doi:10.1038/35055553

Noctor, S. C., Martínez-Cerdeño, V., Ivic, L. and Kriegstein, A. R. (2004). Cortical neurons arise in symmetric and asymmetric division zones and migrate through specific phases. *Nat. Neurosci.* **7**, 136-144. doi:10.1038/nn1172

Nonaka-Kinoshita, M., Reillo, I., Artegiani, B., Martínez-Martínez, M. Á., Nelson, M., Borrell, V. and Calegari, F. (2013). Regulation of cerebral cortex size and folding by expansion of basal progenitors. *EMBO J.* **32**, 1817-1828. doi:10.1038/emboj.2013.96

Otani, T., Marchetto, M. C., Gage, F. H., Simons, B. D. and Livesey, F. J. (2016). 2D and 3D stem cell models of primate cortical development identify species-specific differences in progenitor behavior contributing to brain size. *Cell Stem Cell* **18**, 467-480. doi:10.1016/j.stem.2016.03.003

Papadopoulou, C., Boukakis, G., Ganou, V., Patrinou-Georgoula, M. and Guialis, A. (2012). Expression profile and interactions of hnRNP A3 within hnRNP/mRNP complexes in mammals. *Arch. Biochem. Biophys.* **523**, 151-160. doi:10.1016/j.abb.2012.04.012

Pilaz, L.-J. and Silver, D. L. (2014). Live imaging of mitosis in the developing mouse embryonic cortex. *J. Vis. Exp.* **88**, e51298. doi:10.3791/51298

Pilaz, L.-J., McMahon, J. J., Miller, E. E., Lennox, A. L., Suzuki, A., Salmon, E. and Silver, D. L. (2016). Prolonged mitosis of neural progenitors alters cell fate in the developing brain. *Neuron* **89**, 83-99. doi:10.1016/j.neuron.2015.12.007

Pollen, A. A., Nowakowski, T. J., Chen, J., Retallack, H., Sandoval-Espinosa, C., Nicholas, C. R., Shuga, J., Liu, S. J., Oldham, M. C., Diaz, A. et al. (2015). Molecular identity of human outer radial glia during cortical development. *Cell* **163**, 55-67. doi:10.1016/j.cell.2015.09.004

Pulvers, J. N., Bryk, J., Fish, J. L., Wilsch-Bräuninger, M., Arai, Y., Schreier, D., Naumann, R., Helppi, J., Habermann, B., Vogt, J. et al. (2010). Mutations in mouse Aspm (abnormal spindle-like microcephaly associated) cause not only microcephaly but also major defects in the germline. *Proc. Natl. Acad. Sci. USA* **107**, 16595-16600. doi:10.1073/pnas.1010494107

Rakic, P. (1974). Neurons in rhesus monkey visual cortex: systematic relation between time of origin and eventual disposition. *Science* **183**, 425-427. doi:10.1126/science.183.4123.425

Silbereis, J. C., Pochareddy, S., Zhu, Y., Li, M. and Sestan, N. (2016). The cellular and molecular landscapes of the developing human central nervous system. *Neuron* **89**, 248-268. doi:10.1016/j.neuron.2015.12.008

Smart, I. H. M., Dehay, C., Giroud, P., Berland, M. and Kennedy, H. (2002). Unique morphological features of the proliferative zones and postmitotic compartments of the neural epithelium giving rise to striate and extrastriate cortex in the monkey. *Cereb. Cortex* **12**, 37-53. doi:10.1093/cercor/12.1.37

Sumara, I., Vorlaufer, E., Stukenberg, P. T., Kelm, O., Redemann, N., Nigg, E. A. and Peters, J.-M. (2002). The dissociation of cohesin from chromosomes in prophase is regulated by Polo-like kinase. *Mol. Cell* **9**, 515-525. doi:10.1016/S1097-2765(02)00473-2

Sun, T. and Hevner, R. F. (2014). Growth and folding of the mammalian cerebral cortex: from molecules to malformations. *Nat. Rev. Neurosci.* **15**, 217-232. doi:10.1038/nrn3707

Tanaka, E., Fukuda, H., Nakashima, K., Tsuchiya, N., Seimiya, H. and Nakagama, H. (2007). HnRNP A3 binds to and protects mammalian telomeric repeats in vitro. *Biochem. Biophys. Res. Commun.* **358**, 608-614. doi:10.1016/j.bbrc.2007.04.177

Taverna, E., Götz, M. and Huttner, W. B. (2014). The cell biology of neurogenesis: toward an understanding of the development and evolution of the neocortex. *Annu. Rev. Cell Dev. Biol.* **30**, 465-502. doi:10.1146/annurev-cellbio-101011-155801

Telley, L., Govindan, S., Prados, J., Stevant, I., Nef, S., Dermitzakis, E., Dayer, A. and Jabaudon, D. (2016). Sequential transcriptional waves direct the differentiation of newborn neurons in the mouse neocortex. *Science* **351**, 1443-1446. doi:10.1126/science.aad8361

Telley, L., Agirman, G., Prados, J., Amberg, N., Fièvre, S., Oberst, P., Bartolini, G., Vitali, I., Cadilhac, C., Hippenmeyer, S. et al. (2019). Temporal patterning of apical progenitors and their daughter neurons in the developing neocortex. *Science* **364**, eaav2522. doi:10.1126/science.aav2522

Vargas-Hurtado, D., Brault, J.-B., Piolot, T., Leconte, L., Da Silva, N., Pennetier, C., Baffet, A., Marthiens, V. and Basto, R. (2019). Differences in mitotic spindle architecture in mammalian neural stem cells influence mitotic accuracy during brain development. *Curr. Biol.* **29**, 2993-3005.e9. doi:10.1016/j.cub.2019.07.061

Wang, X., Tsai, J.-W., LaMonica, B. and Kriegstein, A. R. (2011). A new subtype of progenitor cell in the mouse embryonic neocortex. *Nat. Neurosci.* **14**, 555-561. doi:10.1038/nn.2807

Wong, R. W. and Blobel, G. (2008). Cohesin subunit SMC1 associates with mitotic microtubules at the spindle pole. *Proc. Natl. Acad. Sci. USA* **105**, 15441-15445. doi:10.1073/pnas.0807660105

Ye, F., Kang, E., Yu, C., Qian, X., Jacob, F., Yu, C., Mao, M., Poon, R. Y. C., Kim, J., Song, H. et al. (2017). DISC1 regulates neurogenesis via modulating kinetochore attachment of Ndel1/Nde1 during mitosis. *Neuron* **96**, 1041-1054.e5. doi:10.1016/j.neuron.2017.10.010

Yeh, C., Coyaud, E., Bashkurov, M., Van Der Lelij, P., Cheung, S. W. T., Peters, J. M., Raught, B. and Pelletier, L. (2015). The deubiquitinase USP37 regulates chromosome cohesion and mitotic progression. *Curr. Biol.* **25**, 2290-2299. doi:10.1016/j.cub.2015.07.025

Zhang, X., Chen, M. H., Wu, X., Kodani, A., Fan, J., Doan, R., Ozawa, M., Ma, J., Yoshida, N., Reiter, J. F. et al. (2016). Cell-type-specific alternative splicing governs cell fate in the developing cerebral cortex. *Cell* **166**, 1147-1162.e15. doi:10.1016/j.cell.2016.07.025